Contents

Chapter 6

Binaries and stellar evolution

In the next few chapters we will consider evolutionary processes that occur in binary stars. In particular we will address the following questions: (1) Which kinds of interaction processes take place in binaries, and how do these affect their evolution as compared to that of single stars? (2) How do observed types of binary systems fit into the binary evolution scenario?

One type of interaction process was already treated in Chapter 5,[1] namely the dissipative effect of tides which can lead to spin-orbit coupling and to long-term evolution of the orbit (semi-major axis a and eccentricity e). Tidal interaction does not directly affect the evolution of the stars themselves, except possibly through its effect on stellar rotation. In particular it does not change the masses of the stars. However, when in the course of its evolution one of the stars fills its critical equipotential surface, the Roche lobe (Sect. 3.4), mass transfer may occur to the companion, which strongly affects both the masses and evolution of the stars as well as the orbit. Before treating mass transfer in more detail, in this chapter we briefly introduce the concept of Roche-lobe overflow, and give an overview of the aspects of single-star evolution that are relevant for binaries.

6.1 Roche-lobe overflow

The concept of *Roche-lobe overflow* (RLOF) has proven very powerful in the description of binary evolution. The critical equipotential surface in the Roche potential, passing through the inner Lagrangian point L_1, define two Roche lobes surrounding each star (Sect. 3.4). We can define an equivalent radius of the Roche lobe as the radius of a sphere with the same volume, $V_\mathrm{L} = \frac{4}{3}\pi R_\mathrm{L}^3$. Eq. (3.35) provides a fitting formula for the Roche radius of *1 that is accurate to better than 1 % over the entire range of mass ratios $q = M_1/M_2$, i.e.

$$\frac{R_{\mathrm{L},1}}{a} = \frac{0.49q^{2/3}}{0.6q^{2/3} + \ln(1 + q^{1/3})} \tag{6.1}$$

We will often use a somewhat less accurate but simpler fitting formula that is valid for $0.1 < q < 10$:

$$\frac{R_{\mathrm{L},1}}{a} \approx 0.44\frac{q^{0.33}}{(1 + q)^{0.2}} \tag{6.2}$$

Both these expressions are due to P. Eggleton.

Hydrostatic equilibrium in the corotating frame requires that the stellar surface coincides with an equipotential surface. This allows three possible configurations in which both stars are in hydrostatic equilibrium, all of which are observed to occur in nature:

[1] i.e., the articles by Hut (1980, 1981) and Verbunt (2007).

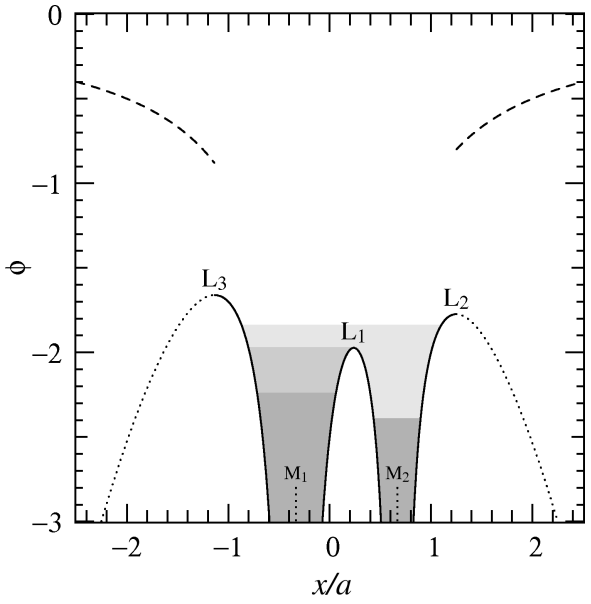

Figure 6.1. Shape of the Roche potential (solid line) along the line connecting the two stars, for a binary with mass ratio $q = M_1/M_2 = 2$. The horizontal scale is in units of the semi-major axis a, and the potential ϕ is in units of $G(M_1 + M_2)/a$. The locations of the centres of mass of the two stars are indicated by M_1 and M_2, and the Lagrangian points by L_1, L_2 and L_3. Gray scales indicate the three possible stable binary configurations: detached (dark), semi-detached (middle) and contact (light gray).

Matter located outside L_2 and L_3 cannot maintain corotation with the orbit, and the Roche potential (shown as dotted lines) loses its physical meaning. Such matter is still bound to the system, as indicated by the dashed lines that represent the gravitational potential of the binary at large distance.

- In a *detached binary* both stars fill an equipotential surface inside their Roche lobes. In this case their structure and evolution is not much affected by the Roche geometry, and can be well approximated by that of single stars.

- If one of the stars exactly fills its Roche lobe while the other is still smaller, the binary is *semi-detached*. If it grows any larger in size the star encounters a 'hole' in its surface equipotential near L_1. This means that hydrostatic equilibrium is no longer possible in the vicinity of the inner Lagrangian point and matter must flow through the nozzle around L_1 into the Roche lobe of its companion (see Chapter 7). This is the idea behind Roche-lobe overflow.

- A final possibility is where both stars fill the same equipotential surface, at a value of the potential above that of L_1 but below that of the outer Lagrangian point L_2 (Fig. 6.1). Such a configuration is known as a *contact binary*, since it requires the stars to be in physical contact. This means that the stars can exchange heat as well as mass, as indeed appears to be the case in observed contact binaries (see a later chapter).

Binaries start out in a detached configuration. As a result of evolution, i.e. expansion due to nuclear evolution of the stars, possibly combined with orbital shrinking owing to angular momentum loss, $R_1/R_{\rm L,1}$ and $R_2/R_{\rm L,2}$ increase with time. A detached binary can thus evolve into a semi-detached binary or, if both stars fill their Roche lobes, into a contact binary.

Three assumptions are made in the Roche geometry (Sect. 3.4), and it is important to reassess them in the context of binary evolution. First, the gravitational fields of both stars are assumed to be those of point masses. This is reasonable, even when stars are filling their Roche lobes, because most stars are very centrally concentrated. Second, the orbit is assumed to be circular. Third, the stellar rotation is assumed to be synchronized with the orbital motion, since the Roche geometry only applies to matter that corotates with the orbit. These last two assumptions are certainly not generally valid, but they are usually satisfied when stars are close to filling their Roche lobes. The reason is that tidal interaction becomes very effective due to its strong dependence on R/a, e.g. in the equilibrium-tide model the circularization timescale depends on $(R/a)^{-8}$ and the synchronization timescale on $(R/a)^{-6}$ (Chapter 5). Both timescales normally become smaller than the stellar expansion timescale when R is close to $R_{\rm L}$.

6.2 Aspects of single-star evolution

6.2.1 Overview

(Adapted from Tauris & van den Heuvel, 2006, Sec. 16.3)

The evolution of a star is driven by a rather curious property of a self-gravitating gas in hydrostatic equilibrium, which is described by the virial theorem. The radiative loss of energy of such a gas sphere causes it to contract and thereby, due to release of gravitational potential energy, to increase its temperature. Thus, while the star tries to cool itself by radiating away energy from its surface, it gets hotter instead of cooler: a star can be said to have a negative heat capacity. The more it radiates to cool itself, the more it will contract, the hotter it gets and the more it is forced to go on radiating. Clearly, this virial cycle is an unstable situation in the long run and explains why a star that starts out as an extended interstellar gas cloud, must finally end its life as a compact object. In the meantime the star spends a considerable amount of time in intermediate stages, during which the radiative energy loss from its surface is compensated by nuclear energy production in its interior, temporarily halting the contraction – a state known as thermal equilibrium. These long-lived stages are known as the main sequence in the case of hydrogen fusion, the horizontal branch in the case of helium fusion, etc. It is important to realize, however, that stars do *not* shine because they are burning nuclear fuel. They shine because they are hot due to their history of gravitational contraction.

Stars that start out with masses $M \lesssim 8\,M_\odot$ suffer from the occurrence of electron degeneracy in their cores at a certain point of evolution. Since for a degenerate gas the pressure depends only on density and not on the temperature, the ignition of a nuclear fuel will not lead to a stabilizing expansion and subsequent cooling. Instead, the sudden temperature rise due to the liberation of energy after ignition causes a runaway nuclear energy production in a so-called 'flash'. In stars with $M \lesssim 2\,M_\odot$ (low-mass stars) the helium core becomes degenerate during hydrogen shell burning on the giant branch and, when its core mass $M_{\rm He}$ reaches $0.47\,M_\odot$, helium ignites with a flash. The helium flash is, however, not violent enough to disrupt the star and it is followed by steady helium burning. Stars with masses in the range $2 \lesssim M/M_\odot \lesssim 8$ (intermediate-mass stars) ignite helium non-degenerately and non-violently. Both low-mass and intermediate-mass stars develop degenerate carbon-oxygen cores after helium burning. Observations of white dwarfs in Galactic clusters that still contain stars as massive as $8^{+3}_{-2}\,M_\odot$ (e.g. Weidemann, 1990) indicate that such massive stars still terminate their life as a white dwarf. They shed their envelopes by a strong stellar wind on the asymptotic giant branch before carbon has a chance to ignite violently.

Table 6.1. End products of stellar evolution as a function of stellar mass, for single stars and for components of close binary stars (roughly, those undergoing case B mass transfer). The columns 'He-core mass' give the maximum mass of the helium core reached by a star of the given initial mass range, for single and close binary stars. The values given are only indicative, and depend on the metallicity (assumed to be solar) and uncertainties in mass loss rates and convective overshooting (mild overshooting was assumed). For binary stars, they also depend on the orbital period and mass ratio.

	single star		close binary star	
initial mass	He-core mass	final remnant	He-core mass	final remnant
$\lesssim 2.0\,M_\odot$	$\approx 0.6\,M_\odot$	CO white dwarf	$< 0.47\,M_\odot$	He white dwarf
$2.0 - 6\,M_\odot$	$0.6 - 1.7\,M_\odot$	CO white dwarf	$0.4 - 1.3\,M_\odot$	CO white dwarf
$6 - 8\,M_\odot$	$1.7 - 2.2\,M_\odot$	ONe white dwarf	$1.3 - 1.7\,M_\odot$	CO white dwarf
$8 - 10\,M_\odot$	$2.2 - 3.0\,M_\odot$	neutron star	$1.7 - 2.2\,M_\odot$	ONe white dwarf
$10 - 25\,M_\odot$	$3.0 - 10\,M_\odot$	neutron star	$2.2 - 8\,M_\odot$	neutron star
$\gtrsim 25\,M_\odot$	$> 10\,M_\odot$	black hole	$> 8\,M_\odot$	neutron star/black hole

A massive star ($M \gtrsim 8\,M_\odot$) evolves through all cycles of nuclear burning alternating with stages of core contraction after exhaustion of nuclear fuel until its core is made of iron, at which point further fusion requires, rather than releases, energy. The core mass of such a star becomes larger than the Chandrasekhar limit, the maximum mass possible for an electron-degenerate configuration ($\approx 1.4\,M_\odot$). Therefore the core implodes to form a neutron star or black hole. The gravitational energy released in this collapse (4×10^{53} erg $\approx 0.15 M_{\rm core} c^2$) is much larger than the binding energy of the stellar envelope, causing the collapsing star to violently explode and eject the outer layers of the star, with a speed of $\sim 10^4$ km/s, in a supernova event. The final stages during and beyond carbon burning are very short-lived ($\lesssim 10^3$ yr) because most of the nuclear energy generated in the interior is liberated in the form of neutrinos which freely escape without interaction with the stellar gas, thereby lowering the outward pressure and accelerating the contraction and nuclear burning.

The possible end-products and corresponding initial masses are listed in Table 6.1. It should be noted that the actual values of the different mass ranges are only known approximately due to considerable uncertainty in our knowledge of the evolution of massive stars. Causes of this uncertainty include limited understanding of the mass loss undergone by stars in their various evolutionary stages. Another fundamental problem is understanding convection, in particular in stars that consist of layers with very different chemical composition. Finally, there is the unsolved question of whether or not the velocity of convective gas cells may carry them beyond the boundary of the region of the star which is convective according to the Schwarzschild criterion. For example, inclusion of this so-called overshooting in evolutionary calculations decreases the lower mass limit for neutron star progenitors (moderate overshooting was assumed in calculating the values in Table 6.1).

Stars in close binary systems can lose their envelope as a result of mass transfer via Roche-lobe overflow, as we shall see in the following chapters. This is the reason why in close binary systems the lower initial mass limits for producing a certain type of remnant are somewhat larger than for an isolated star. Note, however, that the values quoted in Table 6.1 are only indicative and also depend on the orbital period and mass ratio of the binary.

6.2.2 Stellar time scales

Three time scales associated with single stars are important for the study of binary evolution. In order of increasing length these are:

the dynamical time scale This is the time scale on which a star counteracts a perturbation of its hydrostatic equilibrium. It is given by the ratio of the radius of the star R and the average sound velocity of the stellar matter $c_{\rm s}$:

$$\tau_{\rm dyn} = \frac{R}{c_{\rm s}} \approx 0.04 \left(\frac{M_\odot}{M}\right)^{1/2} \left(\frac{R}{R_\odot}\right)^{3/2} \text{ day} \tag{6.3}$$

the thermal or Kelvin-Helmholtz time scale This is the time scale on which a star reacts when energy loss and energy production are no longer in equilibrium. It is given by the ratio of the thermal energy content of the star $E_{\rm th}$ and the luminosity L:

$$\tau_{\rm KH} = \frac{E_{\rm th}}{L} \approx \frac{GM^2}{2RL} \approx 1.5 \times 10^7 \left(\frac{M}{M_\odot}\right)^2 \frac{R_\odot}{R} \frac{L_\odot}{L} \text{ yr} \tag{6.4}$$

the nuclear time scale This is the time scale on which a star uses its nuclear fuel. It is given by the product of the available fusable matter $M_{\rm core}$ and the fusion energy per unit mass Q, divided by the stellar luminosity. For hydrogen fusion with $Q = 0.007c^2$, this is:

$$\tau_{\rm nuc} = 0.007 \frac{M_{\rm core} c^2}{L} \approx 10^{10} \frac{M}{M_\odot} \frac{L_\odot}{L} \text{ yr} \tag{6.5}$$

In the course of its evolution, a star fuses hydrogen in its core on the nuclear time scale. During this time, on the main sequence, the star does not change its radius very much. On the main-sequence we can use the following mass-radius and mass-luminosity relations in eqs. (6.3–6.5):

$$\frac{R}{R_\odot} \simeq \left(\frac{M}{M_\odot}\right)^{0.7} \tag{6.6}$$

$$\frac{L}{L_\odot} \simeq \left(\frac{M}{M_\odot}\right)^{3.8} \tag{6.7}$$

6.2.3 Evolution of the stellar radius and cases of mass transfer

Fig. 6.2a shows evolution tracks in the Hertzsprung-Russell diagram for stars with masses between 1.0 and 25 $M_\odot$, together with lines of constant radius. For three masses (representing low-mass stars, intermediate-mass stars and massive stars, respectively) the corresponding variation of the stellar radius with time is depicted in Fig. 6.2b-d. During the main sequence (central hydrogen burning) phase all stars show a mild increase in radius. Low-mass stars (e.g. the 1.6 $M_\odot$ star) subsequently expand strongly but relatively slowly – on the nuclear timescale of hydrogen-shell burning – during the ascent of the first giant branch, where they develop degenerate helium cores that grow in mass until the occurrence of the helium flash when the core mass $M_c \approx 0.47\,M_\odot$. In contrast, intermediate-mass stars (e.g. the 4 $M_\odot$ star) expand much more rapidly – on a thermal timescale – as they cross the Hertzsprung gap, before they ignite helium non-degenerately. During helium burning low- and intermediate-mass stars describe a loop in the H-R diagram, and their radius remains smaller than it was at the tip of the giant branch. After helium exhaustion in the centre the radius increases again on the asymptotic giant branch, where such stars develop degenerate carbon-oxygen cores. Massive stars (e.g. the 16 $M_\odot$ star) expand more strongly as they cross the Hertzsprung gap and, at least up to about 25 $M_\odot$, burn helium as a red supergiant while their radius keeps expanding slightly. Even more massive stars experience such strong mass loss that their hydrogen-rich envelope is removed by the time helium ignites; their radius decreases and they become Wolf-Rayet stars.

Based on the variation of the stellar radius with time, three cases of mass transfer can be distinguished. An evolving star in a binary can fill its Roche lobe for the first time as it expands on the main sequence (Case A), as it expands after hydrogen exhaustion (Case B), or as it expands after helium exhaustion (Case C). This is depicted in Fig. 6.2b-d for three different masses. Which of the three cases applies depends on the size of the Roche lobe, which in turn depends on the separation between the two stars and (to a lesser extent) on the mass ratio (see eq. 6.1 or 6.2).

The distinction between cases A, B and C contains information about the evolution state of remnant of the donor after mass transfer. Just as important however is a distinction based on the stability of mass transfer. This depends crucially on whether the donor has a radiative or a convective envelope, as will be discussed in Sect. 7.3. The radius at which stars reach the red giant branch and develop a deep convective envelope is also indicated in Fig. 6.2.

Core mass-radius relation for low-mass giants

Low-mass stars on the first giant branch have degenerate helium cores and their luminosity is generated entirely by hydrogen-shell burning around the growing core. The envelope is so extended that it exerts negligible pressure on the dense core, and the luminosity depends only on the mass of the core: low-mass giants follow a very tight core mass-luminosity relation. These stars have deep convective envelopes and are forced to evolve along a Hayashi line[2] at almost constant effective temperature, which only weakly

[2]The Hayashi line is an almost vertical line in the H-R diagram at $T_{\rm eff} \sim 3000$–5000 K that connects fully convective stellar configurations of a certain mass. A star in hydrostatic equilibrium cannot have an effective temperature smaller than that of the

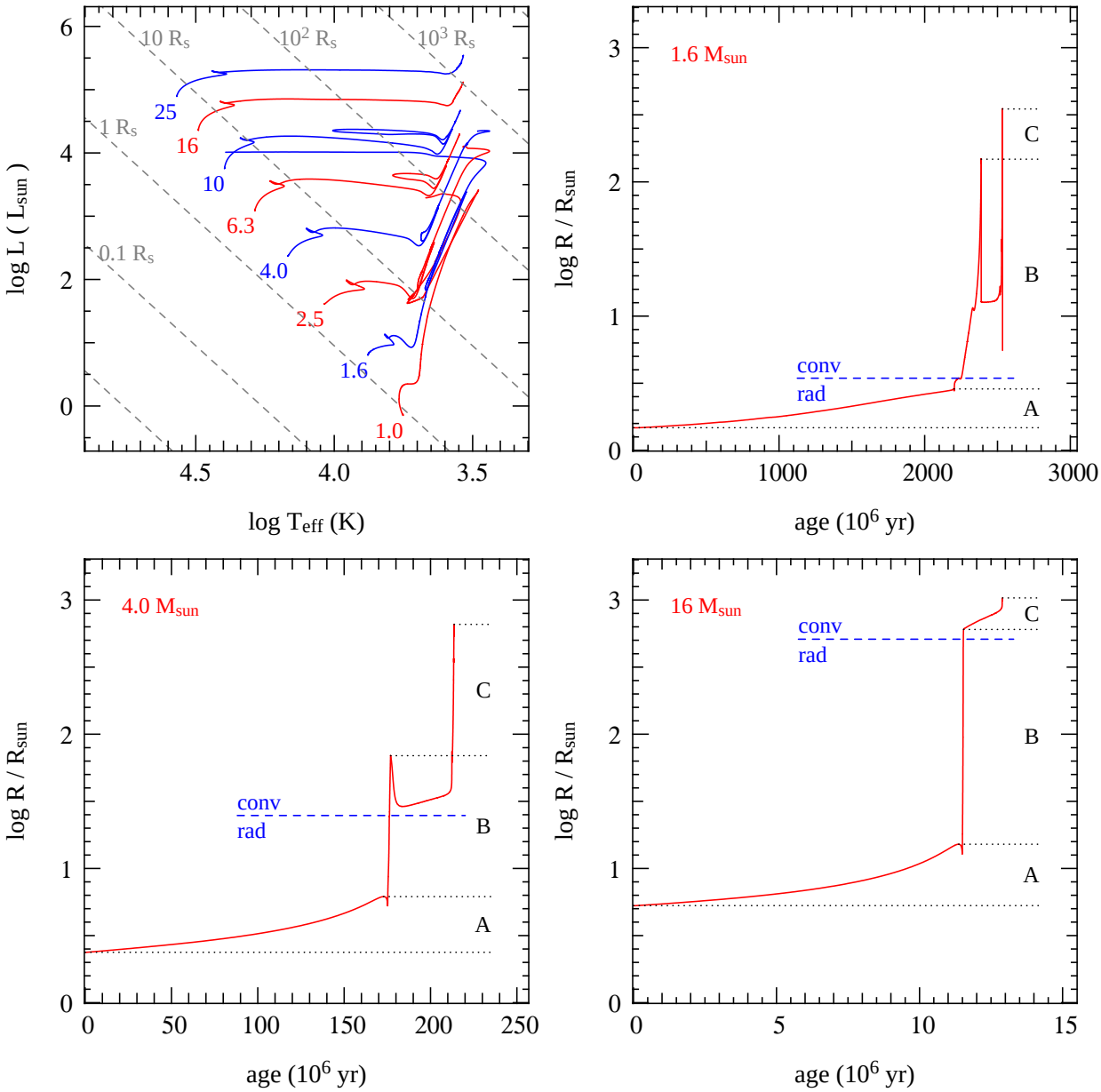

Figure 6.2. Evolution in the H-R diagram (panel a) of single stars with masses between 1.0 and 25 $M_\odot$, as indicated, together with lines of constant radii (in solar radii, dashed lines). The other panels show the variation of the radii of stars of (b) 1.6 $M_\odot$, (c) 4 $M_\odot$ and (d) 16 $M_\odot$ between the ZAMS and either the end of the AGB (1.6 and 4 $M_\odot$) or carbon burning (16 $M_\odot$). The models have been calculated for a metallicity $Z = 0.02$ and a moderate amount of overshooting. The dotted lines indicate the radii at the ZAMS, the end of the MS, the ignition of He, and the maximum radius. The dashed blue line shows the radius at which the stars develop a deep convective envelope on the giant branch.

depends on the mass of the star. Hence there is also a fairly tight core- mass radius relation, as depicted in Fig. 6.3. This relation is very important for low-mass X-ray binaries and certain binary radio pulsars, as we shall see in Chapter 11.

The core-mass radius relation breaks down for masses $\gtrsim 2\,M_\odot$ (the highest mass indicated in Fig. 6.3, as a solid line) and for core masses $\gtrsim 0.47\,M_\odot$ when the radius shrinks in response to helium burning.

Hayashi line appropriate for its mass.

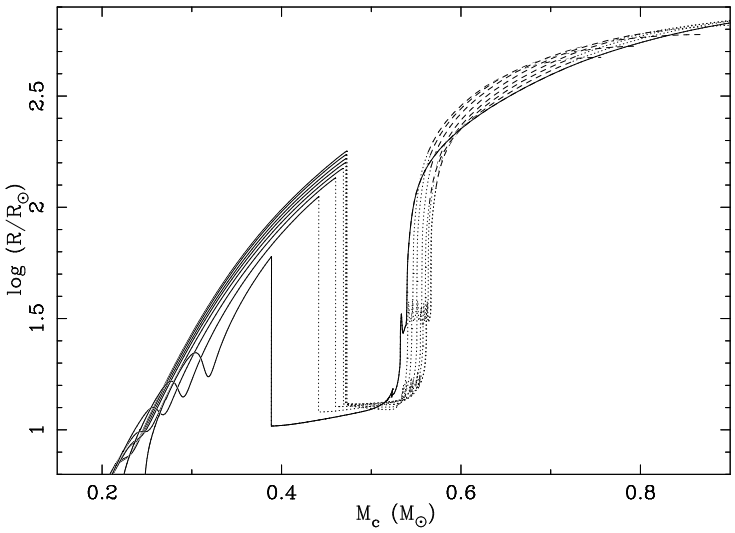

Figure 6.3. Core mass-radius relations for low-mass stars, from detailed stellar models with masses between 0.9 and 2.0 $M_\odot$ computed by van der Sluys et al. (2006). The solid lines correspond to the first giant branch when these stars have a degenerate helium core. The dashed lines show the asymptotic giant branch, with a degenerate carbon-oxygen core. The dotted lines correspond to the core helium-burning phase, when the stellar radius is smaller than the maximum reached on the first giant branch, and during which such stars cannot fill their Roche lobes.

However, for $M_\mathrm{c} \gtrsim 0.6\,M_\odot$ low-mass stars again follow a core mass-radius relation on the asymptotic giant branch.

Exercises

6.1 Show that the ratio of the Roche-lobe radii of binary components is given approximately by

$$\frac{R_{\mathrm{L},1}}{R_{\mathrm{L},2}} \approx q^{0.46} \tag{6.8}$$

for $q = M_1/M_2$ lying between 0.1 and 10.

6.2 For semi-detached binaries there is a relation between the orbital period and the average density of the Roche-lobe filling component, as follows:

$$P = F\left(\frac{\bar{\rho}}{\bar{\rho}_\odot}\right)^{-1/2} \qquad \text{with} \qquad F \approx 0.35\,\mathrm{d}\left(\frac{2}{1+q}\right)^{0.2}, \tag{6.9}$$

where F only depends very weakly on the mass ratio, and can be considered a constant (0.35 d) for practical purposes.

(a) Derive this relation.

(b) Certain 'ultra-compact' binaries have orbital periods of less than 20 minutes. Compare their average density to that of:
- normal main-sequence (MS) stars,
- low-mass helium MS stars, entirely composed of helium, which follow a mass-radius relation $R/R_\odot \approx 0.2(M/M_\odot)$ and have a mass of at least 0.3 $M_\odot$, the minimum mass for helium burning.

(c) What can you conclude about the evolution state of the mass donor in such ultra-compact systems?

6.3 Fig. 6.2c shows how the radius of a star of 4 $M_\odot$ changes during its evolution. Assume such a star has a binary companion of 3 $M_\odot$. Use this plot to calculate:

(a) for which range of orbital periods does mass transfer occur according to case A, case B or case C (determine the transition radii as accurately as possible);

(b) for which orbital periods does the donor star have a radiative envelope.

Chapter 7

Mass transfer in binary stars

A binary system starts out as detached, with both stars in hydrostatic equilibrium and filling an equipotential surface inside their Roche lobes. As a result of evolution, i.e. expansion due to nuclear evolution of the stars, possibly combined with orbital shrinking owing to angular momentum loss, $R_1/R_{\rm L,1}$ and $R_2/R_{\rm L,2}$ increase with time. When one of the stars (usually the most massive star since it has the shortest nuclear timescale) fills its Roche lobe, it encounters a 'hole' in its surface equipotential near L_1. This means that hydrostatic equilibrium is no longer possible in the vicinity of the inner Lagrangian point and matter must flow through the nozzle around L_1 into the Roche lobe of its companion. This is the idea behind Roche-lobe overflow.

In a binary, both stars (*1 and *2) can fill their Roche lobes at subsequent evolutionary stages. We use the convention where *1 denotes the *initially* more massive star of the binary, and *2 the originally less massive star. In this convention the initial mass ratio $q = M_1/M_2 > 1$. During phases of mass transfer we denote the mass-losing star, the *donor*, with subscript 'd' and the companion star, the *accretor*, with subscript 'a' (even if it turns out there is effectively very little or no accretion taking place). Hence the donor can be either *1 or *2, depending on the phase of evolution, but during the first mass transfer phase the donor will always be *1.

7.1 The rate of mass transfer by Roche-lobe overflow

Mass flow through the inner Lagrangian point is, in all its generality, a rather complicated hydrodynamical problem. In the following we will make it plausible that the rate of mass transfer through L_1 depends very sensitively on the fractional radius excess of the donor, $\Delta R/R_{\rm L} = (R_{\rm d} - R_{\rm L})/R_{\rm L}$. This allows a great simplification of the problem in many practical applications.

The rate of mass flow $\dot{M}$ can be written as the product of the density ρ and the velocity v of the gas at L_1, and the cross section S of the stream,

$$\dot{M} \approx (\rho v)_{L_1} \cdot S \tag{7.1}$$

To estimate S consider the Roche potential in the plane through L_1 perpendicular to the line connecting both stars, i.e. in the plane $x = 0$. In the vertical (y) direction the potential has a roughly parabolic shape as follows from the Taylor expansion

$$\Delta\phi \equiv \phi(x,y) - \phi(x,0) = \frac{\partial\phi}{\partial y}\Big|_{L_1} y + \tfrac{1}{2}\frac{\partial^2\phi}{\partial y^2}\Big|_{L_1} y^2 \tag{7.2}$$

$$\approx \tfrac{1}{2}\omega^2 y^2 \tag{7.3}$$

The first derivative of ϕ is zero since $(x,y) = (0,0)$ corresponds to a saddle point in the potential. Furthermore it can be shown, from the definition of the Roche potential in combination with Kepler's law,

that to within a factor of order unity $(\partial^2\phi/\partial y^2)|_{L_1} \approx \omega^2$ where ω is the orbital frequency, which gives the second equation. This is interpreted as follows: the amount $\Delta\phi$ by which the surface potential of the donor exceeds the critical potential, is approximately ω^2 times the cross section y^2 of the stream passing through L_1. By considering a point on the surface of the donor far away from L_1, where the potential is roughly spherical and dominated by the gravitational potential, $\phi \approx -GM_\mathrm{d}/R_\mathrm{d}$, we also obtain

$$\Delta\phi \approx \frac{GM_\mathrm{d}}{R_\mathrm{d}}\frac{\Delta R}{R} \qquad \Rightarrow \qquad S \approx y^2 \approx \frac{GM_\mathrm{d}}{\omega^2 R_\mathrm{d}}\frac{\Delta R}{R} \tag{7.4}$$

The product ρv can be estimated by considering that at L_1 the gas expands freely into the Roche lobe of the companion, so that the velocity is given by the local sound speed $c_\mathrm{s} = \sqrt{P/\rho}$. We can eliminate ρ by considering the equation of state, approximated by the polytropic relation $P = K\rho^\gamma$. This gives $c_\mathrm{s} = \sqrt{K\rho^{\gamma-1}}$ and hence $\rho \propto {c_\mathrm{s}}^{2/(\gamma-1)}$, so that

$$(\rho v)_{L_1} \propto {c_\mathrm{s}}^{\frac{\gamma+1}{\gamma-1}}$$

Finally, at L_1 the kinetic energy in the stream should equal the potential difference across it, i.e. $\frac{1}{2}v^2 = \Delta\phi$ which gives us $c_\mathrm{s} \approx v \propto \sqrt{\Delta R/R}$ from eq. 7.4. With both ρv and S now expressed in terms of $\Delta R/R$ we arrive at a dimensional relation between $\dot{M}$ and $\Delta R/R$:

$$\dot{M} \propto \left(\frac{\Delta R}{R}\right)^{\frac{3\gamma-1}{2\gamma-2}}$$

For stars with convective envelopes, i.e red giants or low-mass main-sequence stars, $\gamma = \frac{5}{3}$ and the value of the exponent equals 3. However, any other reasonable value of γ also yields a strong dependence of $\dot{M}$ on $\Delta R/R$.

A more detailed derivation applying Bernoulli's law to the gas flow through the nozzle around L_1 yields the following equation:

$$\dot{M} = -A\frac{M_\mathrm{d}}{P}\left(\frac{\Delta R}{R}\right)^3 \tag{7.5}$$

where M_d is the donor mass, P the orbital period and A is a numerical constant of order ∼10. This relation implies that (1) the mass transfer rate is highly sensitive to the radius excess, with a slowly increasing $\Delta R/R$ leading to strongly increasing $\dot{M}$, and (2) even a modest radius excess of say 10 % would lead to an enormous mass transfer rate and to the transfer of the entire donor mass in about a hundred orbits. In practice this means that for relatively slow, steady mass transfer, such as is observed semi-detached binaries, the donor only overfills its Roche radius by a small fraction. This can be seen by writing eq. (7.5) as

$$\frac{\Delta R}{R} \sim \left(\frac{\dot{M}}{M}P\right)^{1/3} = \left(\frac{P}{\tau_{\dot{M}}}\right)^{1/3} \tag{7.6}$$

where $\tau_{\dot{M}}$ is the timescale of mass transfer. For mass transfer occurring on the nuclear timescale or even on the thermal timescale of the donor (see Sect. 6.2.2) this yields $\Delta R/R_\mathrm{d} < 0.01$. Hence, unless mass transfer is much more rapid than the thermal timescale of the donor, it is a very good approximation to take $R_\mathrm{d} = R_\mathrm{L}$.

7.2 Orbital evolution during mass transfer

In Chapter 2 the orbital angular momentum per unit reduced mass, $l = J/\mu$, of a binary was derived. Hence the orbital angular momentum J of a binary is given by

$$J^2 = G\,\frac{{M_1}^2{M_2}^2}{M_1 + M_2}\,a(1-e^2). \tag{7.7}$$

In many cases the angular momentum stored in the rotation of the two stars is negligible compared to the orbital angular momentum, so that eq. (7.7) also represents the total angular momentum of the binary, to good approximation. By differentiating this expression we obtain a general equation for orbital evolution:

$$2\frac{\dot{J}}{J} = \frac{\dot{a}}{a} + 2\frac{\dot{M}_1}{M_1} + 2\frac{\dot{M}_2}{M_2} - \frac{\dot{M}_1 + \dot{M}_2}{M_1 + M_2} - \frac{2e\,\dot{e}}{1-e^2}. \tag{7.8}$$

In the case of Roche-lobe overflow in an already circularized binary, the last term is zero. The $\dot{J}$ term represents angular momentum loss from the binary, which can be due to spontaneous processes (such as gravitational wave radiation) or it can be associated with mass loss from the binary as a whole or from the component stars. In the latter case $\dot{J}$ is related to the $\dot{M}$ terms.

7.2.1 Conservative mass transfer

We first consider *conservative mass transfer*, in which the total mass and orbital angular momentum of the binary are conserved. In that case we can set

$$\dot{J} = 0 \qquad \text{and} \qquad \dot{M}_\mathrm{a} = -\dot{M}_\mathrm{d},$$

and eq. (7.8) reduces to

$$\frac{\dot{a}}{a} = 2\left(\frac{M_\mathrm{d}}{M_\mathrm{a}} - 1\right)\frac{\dot{M}_\mathrm{d}}{M_\mathrm{d}}. \tag{7.9}$$

Eq. (7.9) tells us that, because $\dot{M}_\mathrm{d} < 0$, the orbit shrinks ($\dot{a} < 0$) as long as $M_\mathrm{d} > M_\mathrm{a}$ and the orbit expands when $M_\mathrm{d} < M_\mathrm{a}$. In other words, the minimum separation for conservative mass transfer occurs when $M_\mathrm{d} = M_\mathrm{a}$. An explicit relation between the separation and the masses can be found by integrating eq. (7.9), or more directly from eq. (7.7) with $e = 0$:

$$M_\mathrm{d}^2\, M_\mathrm{a}^2\, a = \text{constant}, \qquad \text{or} \qquad \frac{a}{a_\mathrm{i}} = \left(\frac{M_\mathrm{d,i}}{M_\mathrm{d}}\frac{M_\mathrm{a,i}}{M_\mathrm{a}}\right)^2 \tag{7.10}$$

The index 'i' denotes the initial value. We can use Kepler's law to obtain similar relations between the rate of change of the orbital period $\dot{P}$ and the rate of mass transfer $\dot{M}_\mathrm{d}$, and between the period and masses directly:

$$\frac{\dot{P}}{P} = 3\left(\frac{M_\mathrm{d}}{M_\mathrm{a}} - 1\right)\frac{\dot{M}_\mathrm{d}}{M_\mathrm{d}}, \qquad \text{and} \qquad \frac{P}{P_\mathrm{i}} = \left(\frac{M_\mathrm{d,i}}{M_\mathrm{d}}\frac{M_\mathrm{a,i}}{M_\mathrm{a}}\right)^3 \tag{7.11}$$

The usefulness of the first equation is that it allows a determination of the mass transfer rate of observed semi-detached binaries, if the masses and the period derivative can be measured (and if the assumption of conservative mass transfer is valid). This is complicated by the fact that many binaries show short-term period fluctuations, while what is needed is the long-term average of the period derivative. However, for some binaries this long-term trend has been determined with reasonable accuracy.

7.2.2 Non-conservative mass transfer and mass loss

The assumption of conservation of total mass and angular momentum is a useful idealization, but it cannot be expected to hold in many circumstances. This is unfortunate because the situation becomes much more complicated and uncertain when mass and angular momentum loss from the binary have to be considered. Observationally there is evidence for both conservatively and non-conservatively evolving binaries, as we will discuss later. For now we will just derive some useful expressions for orbital evolution, in which mass and angular momentum loss are simply parameterized. These can also be applied

to the situation where one or both of the stars is losing mass by a stellar wind, in the absence of mass transfer.

Suppose that only a fraction β of the transferred mass is accreted by the companion star, so that

$$\dot{M}_\mathrm{a} = -\beta \dot{M}_\mathrm{d} \qquad \text{and} \qquad \dot{M}_\mathrm{a} + \dot{M}_\mathrm{d} = (1-\beta)\dot{M}_\mathrm{d}.$$

We also need to specify how much angular momentum is taken away by the matter that is lost from the binary. This can be parameterized in different ways, here we will take the specific angular momentum of the ejected matter to be γ times the specific angular momentum of the binary, i.e.

$$h_\mathrm{loss} \equiv \frac{\dot{J}}{\dot{M}_\mathrm{a} + \dot{M}_\mathrm{d}} = \gamma \frac{J}{M_\mathrm{a} + M_\mathrm{d}} \tag{7.12}$$

so that in eq. (7.8) we can replace the $\dot{J}$ term by

$$\frac{\dot{J}}{J} = \gamma(1-\beta)\frac{\dot{M}_\mathrm{d}}{M_\mathrm{d} + M_\mathrm{a}} \tag{7.13}$$

We can now derive an expression for the change in separation resulting from non-conservative mass transfer:

$$\frac{\dot{a}}{a} = -2\frac{\dot{M}_\mathrm{d}}{M_\mathrm{d}}\left[1 - \beta\frac{M_\mathrm{d}}{M_\mathrm{a}} - (1-\beta)(\gamma + \tfrac{1}{2})\frac{M_\mathrm{d}}{M_\mathrm{d} + M_\mathrm{a}}\right] \tag{7.14}$$

Note that the difficulty is in specifying β and γ, or rather, how these parameters depend on say the masses of the stars and on the details of the mass transfer process. We will address some of these problems later.

For some (still idealized) physical situations at least γ can be specified in terms of other quantities. Several 'modes' of non-conservative mass mass transfer can be considered:

Fast mode or Jeans mode If mass is lost from the donor star in the form of a fast isotropic wind, it will simply take away the specific orbital angular momentum of the donor in its relative orbit around the centre of mass, with $a_\mathrm{d} = a\, M_\mathrm{a}/(M_\mathrm{d} + M_\mathrm{a})$. The assumption of a fast wind implies that the ejected matter does not interact with the binary system, and a further assumption is that the physical size of the star is neglected so that it is treated as a point mass. Then the specific angular momentum of the wind matter is

$$h_\mathrm{loss} = a_\mathrm{d}^2\omega = \left(\frac{M_\mathrm{a}}{M_\mathrm{d} + M_\mathrm{a}}\right)^2 \sqrt{G(M_\mathrm{d} + M_\mathrm{a})\, a} \tag{7.15}$$

which can be verified to correspond to $\gamma = M_\mathrm{a}/M_\mathrm{d}$.

Isotropic re-emission Another physical situation that may arise is when mass is actually transferred to the companion by RLOF, but only part of this matter is accreted with the rest being ejected isotropically from the close vicinity of the accreting star. This can be the case when mass accretion drives an enhanced stellar wind from the accretor, or when the excess mass is ejected in the from of jets from a compact object. In that case $h_\mathrm{loss} = a_\mathrm{a}^2\omega$ which corresponds to $\gamma = M_\mathrm{d}/M_\mathrm{a}$.

Circumbinary ring The last situation, also sometimes called the 'intermediate mode', is when the mass that is lost is not ejected from the potential of the binary but forms a ring around the system. This may occur when a contact binary is formed and the critical potential surface corresponding to the outer Lagrangian point L_2 is reached. Mass will then be lost through L_2 without having enough energy to escape (see Fig. 6.1), and it may end up in a Keplerian orbit around the binary at some distance a_ring from the centre of mass. Then the specific angular momentum of such a ring will be

$$h_\mathrm{ring} = [G(M_\mathrm{d} + M_\mathrm{a})\, a_\mathrm{ring}]^{1/2} \tag{7.16}$$

which corresponds to

$$\gamma = \frac{(M_\mathrm{d} + M_\mathrm{a})^2}{M_\mathrm{d} M_\mathrm{a}} \sqrt{\frac{a_\mathrm{ring}}{a}} \tag{7.17}$$

A more detailed description of orbital evolution according to these modes, as well as for a combination of several modes, can be found in the paper by Soberman et al. (1997). Beware, however, that a different notation is used in that paper.

7.3 Stability of mass transfer

When Roche-lobe overflow starts, the stability of the mass transfer process and its consequences depend on (1) how the radius of the donor responds to the imposed mass loss, and (2) how the orbit (and therefore R_L) responds to mass transfer. Once mass transfer is initiated its development and outcome also depend on (3) the response of the companion star to the mass that is being transferred to it. We defer this last issue to a later section, and for now assume the accreting star is an inert point mass and consider only the effect on the donor star.

We can derive *stability criteria* for the onset of mass transfer by considering points (1) and (2). We do this by comparing the stellar radius to the Roche radius as a function of decreasing donor mass in the *R*-*M* diagram, as depicted schematically in Fig 7.1a. The diagram shows the Roche radius of the donor star for conservative mass transfer in a binary with total mass $2\,M_\odot$, and two examples of evolution tracks, for initial donor masses $1.0\,M_\odot$ (starting at point A) and $1.4\,M_\odot$ (starting at point D). The stars evolve vertically upwards in this diagram (nuclear expansion at constant mass) until the onset of RLOF

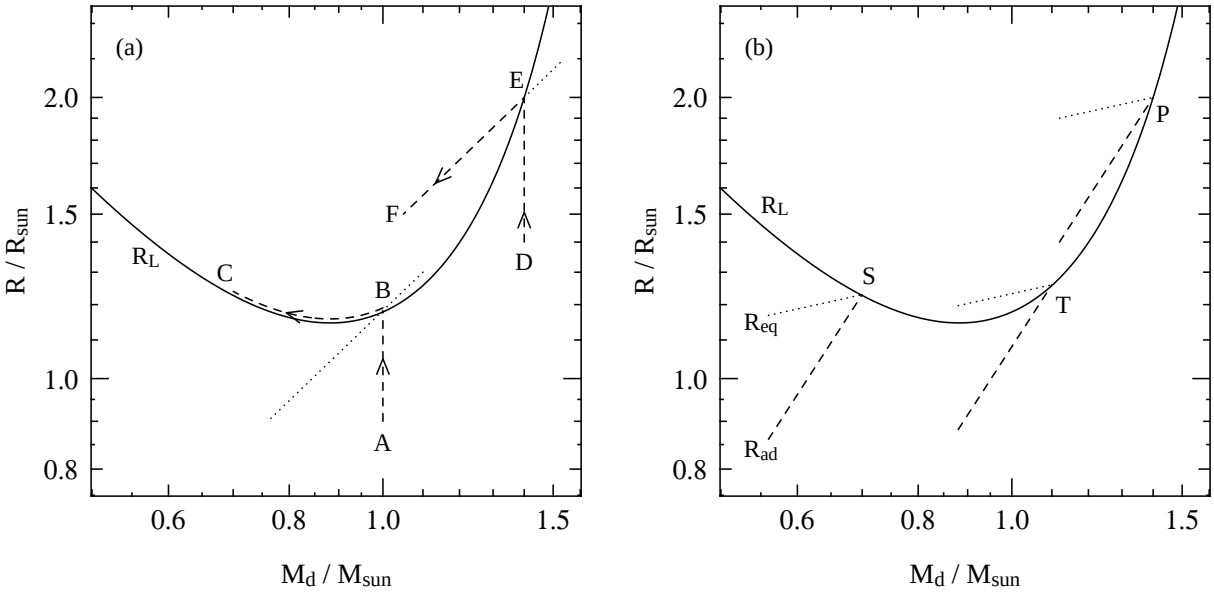

Figure 7.1. (a) Schematic behaviour of the Roche radius (solid line) and stellar radius (dashed lines, for two cases) as functions of the donor mass. The Roche radius curve is drawn for conservative mass transfer in a binary with total mass $2\,M_\odot$. The dotted lines show a fiducial stellar mass-radius relation, for the purpose of this example taken as $R \propto M$ (i.e. $\zeta_* = 1$). See test for discussion. (b) The solid curve is the same Roche radius as in panel a, but now the dashed and dotted lines indicate schematically the adiabatic (R_ad) and thermal-equilibrium (R_eq) responses of the donor to mass loss, respectively (for the purpose of illustration it is assumed that $\zeta_\mathrm{ad} = 1.5$ and $\zeta_\mathrm{eq} = 0.25$). Mass transfer starting at S, T and P correspond to stable, thermal-timescale and dynamically unstable mass transfer respectively, as discussed in the text.

at point B and E, respectively, when $R_d = R_L$. Upon mass loss the donor radius may behave as given by the dotted lines through points B and E. After a small amount of mass loss, $\delta M < 0$, we look at the quantity $\delta R = R_d - R_L$ and we can have either that $R_d \leq R_L$ ($\delta R \leq 0$, e.g. point B in Fig 7.1a) or $R_d > R_L$ ($\delta R > 0$, e.g. point E). In the first case, the donor detaches from its Roche lobe and it has to re-expand before RLOF can continue. Obviously this is the condition for stable mass transfer. In this case it is nuclear expansion that makes the donor continue to fill its Roche lobe and to drive mass transfer, and the stellar radius follows path B-C. In the second case ($\delta R > 0$) the mass transfer rate – which depends very strongly on $\delta R/R$ as shown in Sect. 7.1 – increases, leading to even more mass loss and a larger δR (path E-F in Fig 7.1a). This is a runaway situation, leading to unstable mass transfer. It thus appears that we have to compare the slope of the mass-radius relation, of both the stellar radius and the Roche radius. These slopes are expressed by the so-called mass-radius exponents,

$$\zeta_* \equiv \frac{d\log R_d}{d\log M}, \qquad \zeta_L \equiv \frac{d\log R_L}{d\log M}, \tag{7.18}$$

where $\zeta_* \geq \zeta_L$ implies stability and $\zeta_* < \zeta_L$ implies instability of RLOF. The situation is complicated, however, by the fact that stars react to perturbations (like mass loss) on two very different timescales.

If a star suddenly loses mass both its hydrostatic equilibrium and its thermal equilibrium will be disturbed. The star reacts by readjusting its structure and thereby its radius in order to recover equilibrium. Since hydrostatic readjustment happens on the star's dynamical timescale, which is much shorter than the Kelvin-Helmholtz timescale on which it readjusts thermally, the initial (dynamical) response to mass loss will be almost adiabatic. For the question of the *dynamical stability* of mass transfer we must thus consider the *adiabatic* response of the stellar radius to mass loss. This can be expressed as $(\delta R/R)_{ad} = \zeta_{ad}\,\delta M/M$, i.e. we define the adiabatic mass-radius exponent,

$$\zeta_{ad} \equiv \left(\frac{d\log R}{d\log M}\right)_{ad}. \tag{7.19}$$

The criterion for dynamical stability of mass transfer then becomes $\zeta_{ad} \geq \zeta_L$.

If this criterion is fulfilled, then the donor will shrink within its Roche lobe on a dynamical timescale and is able to recover hydrostatic equilibrium. In that case the slower thermal readjustment of the donor becomes relevant. On the Kelvin-Helmholtz timescale the star will attempt to recover the thermal equilibrium radius appropriate for its new mass $M + \delta M(< M)$, and the change in its equilibrium radius can be expressed as $(\delta R/R)_{eq} = \zeta_{eq}\,\delta M/M$ or

$$\zeta_{eq} \equiv \left(\frac{d\log R}{d\log M}\right)_{eq}. \tag{7.20}$$

If, in addition to $\zeta_{ad} \geq \zeta_L$, also $\zeta_{eq} \geq \zeta_L$ then the new equilibrium radius will be smaller than the Roche radius, and we have the condition for *secularly stable* mass transfer. In the intermediate case, $\zeta_{ad} \geq \zeta_L > \zeta_{eq}$, thermal readjustment of the donor keeps pushing it to overfill its Roche lobe. Mass transfer then occurs on the donor's thermal timescale as discussed below.

Based on the above stability considerations we can distinguish three cases of mass transfer, corresponding to different timescales, which are illustrated schematically in Fig 7.1b. (This classification is independent of the division into cases A, B and C discussed before!)

Case 1: stable mass transfer if $\zeta_L \leq \min(\zeta_{ad}, \zeta_{eq})$

This corresponds to mass transfer starting at point S in Fig 7.1b. The donor remains in thermal equilibrium, and continuing mass transfer is driven either by nuclear evolution of the donor (expansion, i.e. R_{eq} increases with time) or by orbital shrinkage due to angular momentum loss ($R_L$decreases). Mass transfer thus occurs on the nuclear timescale of the donor, or on the timescale for angular momentum loss, whichever is shorter.

Case 2: thermal-timescale mass transfer if $\zeta_{\rm ad} \geq \zeta_{\rm L} > \zeta_{\rm eq}$

Mass transfer is dynamically stable, but driven by thermal readjustment of the donor. This corresponds to mass transfer starting at point T in Fig 7.1b. Initially the mass transfer rate increases, but then saturates at a value determined by the donor's thermal timescale:

$$\dot{M}_{\rm max} \approx -M_{\rm d}/\tau_{\rm KH,d} \tag{7.21}$$

This case is sometimes called 'thermally unstable' mass transfer but this is misleading: despite the thermal disequilibrium of the donor, mass transfer is stable and *self-regulating*. If $\dot{M}$ were smaller than eq. (7.21) the donor would be allowed to expand to regain equilibrium, leading to an increasing mass transfer rate. On the other hand if $\dot{M}$ were much larger the donor would react almost adiabatically and shrink inside its Roche lobe. The radius excess $\delta R/R$ adjusts itself to maintain the thermal-timescale mass loss rate. As shown in Sect. 7.1, this implies $\delta R/R < 0.01$. Hence also in this case, the donor radius closely follows the Roche radius, but $R_{\rm d} < R_{\rm eq}$.

Case 3: dynamically unstable mass transfer if $\zeta_{\rm L} > \zeta_{\rm ad}$

This corresponds to mass transfer starting at point P in Fig 7.1b. The adiabatic response of the donor is unable to keep it within its Roche lobe, leading to ever-increasing mass-transfer rates. As discussed above this is an unstable, runaway situation. Detailed calculations show that mass transfer accelerates to a timescale in between the thermal and dynamical timescale of the donor. This has dramatic effects on the evolution of the binary, probably leading to a common-envelope situation (Sect. 10.2).

For these criteria to be of practical use, we need to consider how the various ζ's depend on the properties of the binary system and on the mass and evolution state of the donor.

7.3.1 Response of the Roche radius to mass loss

The example shown in Fig 7.1 indicates that the reaction of the Roche radius depends primarily on the binary mass ratio. This can be easily shown for the case of conservative mass transfer, for which (see Exercise 7.1)

$$\zeta_{\rm L} = 2.13q - 1.67, \qquad \text{for } q = M_{\rm d}/M_{\rm a} < 10. \tag{7.22}$$

The important consequence of this expression is that the stability criteria for mass transfer can be rewritten in terms of a critical mass ratio (see § 7.3.3 below). However, it is important to realize that $\zeta_{\rm L}$ can take on different values for non-conservative mass transfer, i.e. it depends on the mode of mass and angular-momentum loss, as well as on the mass ratio. For a particular mode, such as those discussed in Sect. 7.2.2, the dependence of $\zeta_{\rm L}$ on mass ratio can be derived (see the article by Soberman et al., 1997).

7.3.2 Response of the stellar radius to mass loss

The adiabatic response of a star to mass loss, and hence the value of $\zeta_{\rm ad}$, depends critically on the structure of its envelope, in particular on whether the envelope is convective or radiative. Detailed calculations show that stars with radiative envelopes shrink rapidly in response to mass loss (i.e. $\zeta_{\rm ad} \gg 0$), while stars with convective envelopes tend to expand or keep a roughly constant radius ($\zeta_{\rm ad} \lesssim 0$).

We can make this plausible by recalling the criterion for convection to occur. If a gas element is displaced upwards adiabatically from its equilibrium position, while maintaining pressure equilibrium with its surroundings, it will experience an upward buoyancy force if its density is smaller than that of its surroundings. The envelope is then unstable to convective motions, which efficiently redistribute energy so as to make the envelope structure nearly adiabatic. This means that $P \propto \rho^{\gamma_{\rm ad}}$, i.e. the density

within a convective envelope falls off with pressure as $\rho \propto P^{1/\gamma_{\rm ad}}$. On the other hand, if the envelope is stable against convection, the density gradient must necessarily be steeper than adiabatic in order for the buoyancy force on a displaced gas element to restore it to its original position. This means that radiative envelopes are more centrally concentrated than convective envelopes, and have relatively low density in the outer layers. When the outermost layers of a star are suddenly removed by mass loss, the layers below it are decompressed and will expand adiabatically to restore pressure equilibrium. For a convective envelope that is already adiabatically stratified, we may therefore expect that the density distribution (measured at constant pressure) will remain the same, and the star will therefore occupy about the same volume when hydrostatic equilibrium is restored. In other words, $R_{\rm ad}$ is insensitive to mass loss. On the other hand, the steeper initial density profile in a radiative envelope means that, first of all, the layers exposed by mass loss lie deeper within the star. After adiabatic expansion, the outer layers will furthermore have a higher density when measured at constant pressure. Therefore when hydrostatic equilibrium is restored, a star with a radiative envelope will occupy a *smaller* volume and have a smaller radius.

This expectation is borne out by more detailed considerations. For an ideal monatomic gas, $\gamma_{\rm ad} = \frac{5}{3}$, and a convective envelope behaves like an $n = \frac{3}{2}$ polytrope. Stars whose entire structure is described by an $n = \frac{3}{2}$ polytrope, such as white dwarfs and completely convective stars, follow a mass-radius relation $R \propto M^{-1/3}$, i.e. they expand upon mass loss and $\zeta_{\rm ad} = -\frac{1}{3}$. This is relevant for low-mass main-sequence stars with $M \lesssim 0.35\,M_\odot$ which are completely convective. Evolved stars on the red giant branch have deep convective envelopes and a dense core, these can be described by so-called condensed polytropes. The response of such models to mass loss was studied by Hjellming & Webbink (1987) who found $\zeta_{\rm ad}$ to increase with the fractional mass of the dense core, turning positive for $M_{\rm c} > 0.2M$; see Fig. 1 of Soberman et al. (1997) who also provide a convenient fitting formula, eq. (60). To summarize, stars with deep convective envelopes respond to mass loss by either expanding or keeping their radius roughly constant. This has important consequences for mass transfer from red giants.

The equilibrium radius response to mass loss also depends on the evolution state of the donor, but in a different way. For homogeneous stars, i.e. stars on the zero-age main sequence, $R_{\rm eq}$ is simply given by their mass-radius relation. Hence for upper ZAMS stars ($M \gtrsim 1\,M_\odot$) we have $\zeta_{\rm eq} \approx 0.6$ and for low-mass ZAMS stars ($M \lesssim 1\,M_\odot$) $\zeta_{\rm eq} \approx 1.0$. However for stars that are more evolved, and have a non-homogeneous composition profile, we cannot simply apply the MS mass-radius relation. We need to consider the response on a timescale that is much slower than thermal, so that the star remains in TE, but faster than the nuclear timescale, so that the composition profile does not change. The effect of a non-homogeneous composition is to make stars expand rather than contract in response to mass loss, as is borne out by detailed calculations. Hence $\zeta_{\rm eq} \lesssim 0$ for fairly evolved MS stars. Detailed calculations also show that for stars in post-MS phases, the equilibrium radius is insensitive to the total stellar mass, hence $\zeta_{\rm eq} \approx 0$. On the other hand, for low-mass red giants the radius depends strongly on the *core* mass, see Sect. 6.2.3.

Finally, for white dwarfs the response is again given by their mass-radius relation, i.e. $\zeta_{\rm eq} = -\frac{1}{3}$. For these degenerate configurations there is no distinction between the adiabatic and thermal response.

7.3.3 Consequences for binary evolution

The stability criteria discussed above translate, with the use of eq. (7.22), into critical mass ratios for the stability of (conservative) mass transfer. Since the initial mass ratio $q = M_{\rm d}/M_{\rm a} > 1$, the initial value of $\zeta_{\rm L}$ is always > 0.46. Stars with deep convective envelopes, i.e. red giants and red supergiants, have $\zeta_{\rm ad} \lesssim 0$, so the first stage of mass transfer from such donors will always be dynamically unstable. Comparison with Fig 6.2 shows that Case C mass transfer is always expected to be dynamically unstable, as well as Case B mass transfer in low-mass binaries and late Case B mass transfer in intermediate-mass

binaries, with RLOF starting on the first giant branch. Dynamically unstable mass transfer can only be avoided in these binaries if stellar-wind mass loss reduces the donor mass to well below the accretor mass, so that $q \lesssim 0.8$ when RLOF starts.

For donors with radiative envelopes, having $\zeta_{\rm ad} \gg 0$, RLOF will only be dynamically unstable if the donor is much more massive than the accretor. For $q \lesssim 4$ mass transfer is dynamically stable and usually occurs on the thermal timescale, since for practically all stars $\zeta_{\rm eq} \lesssim 0$. Only if the donor fills its Roche lobe very close to the ZAMS ($\zeta_{\rm eq} \approx 0.6 - 1.0$) in a very close binary with nearly equal masses, can one expect stable (nuclear-timescale) mass transfer. Therefore thermal-timescale mass transfer should occur in most Case A binaries, as well as early Case B binaries of intermediate and high mass with periods such that mass transfer occurs during the Hertzprung-gap expansion of the donor.

Exercises

7.1 Using the approximate expression (6.2) for the Roche-lobe radius of the donor, show that for conservative mass transfer the rate of change of $R_{\rm L}$ is given by

$$\frac{\dot{R}_{\rm L}}{R_{\rm L}} = \left(2.13\frac{M_{\rm d}}{M_{\rm a}} - 1.67\right)\frac{\dot{M}_{\rm d}}{M_{\rm d}} \tag{7.23}$$

and that $R_{\rm L}$ has a minimum for $M_{\rm d} \approx 0.78 M_{\rm a}$.

7.2 β Lyrae is a semi-detached eclipsing binary in which the orbital period has been observed to change over the last 100 years. The observed ephemeris (the time of primary eclipse as a function of orbital cycle) is quite accurately fitted by a parabolic expression:

$$T_{\rm prim.eclipse}({\rm d}) = {\rm JD}2408247.966 + 12.913780\,E + 3.87196 \times 10^{-6}\,E^2$$

where E counts the number of eclipses.

(a) Derive the orbital period of β Lyr and the rate of change of its orbital period.

(b) From the radial velocity variations the masses of the components have been measured as $M_1 \sin^3 i = 12.94 \pm 0.05\,M_\odot$ and $M_2 \sin^3 i = 2.88 \pm 0.10\,M_\odot$. The inclination is not accurately measured, however. Assuming conservative mass transfer is taking place, calculate the mass transfer rate and estimate its uncertainty.

7.3 Show that in a binary system in which one star is losing mass in a fast, isotropic stellar wind, the separation relates to the total binary mass as

$$a\,(M_1 + M_2) = \text{constant} \tag{7.24}$$

if the finite dimensions of the star are ignored (i.e. it is treated as a point mass).

This result implies that if one or both stars are losing mass, the binary separation increases (inversely with total mass) even though the angular momentum decreases.

7.4 Derive the following expression for the mass transfer rate for stable (nuclear-timescale) mass transfer, in terms of the mass mass-radius exponents $\zeta_{\rm L}$ and $\zeta_{\rm eq}$ and the rate at which the stellar (equilibrium) radius would change in the absence of mass loss, $(\partial R_{\rm eq}/\partial t)_M$:

$$\dot{M}_{\rm d} = -\frac{M_{\rm d}}{\zeta_{\rm eq} - \zeta_{\rm L}}\left(\frac{\partial \ln R_{\rm eq}}{\partial t}\right)_M \tag{7.25}$$

(Hint: write $\dot{R} = dR/dt$ in terms of the partial derivatives with respect to t and M, and use the condition that the donor star just keeps filling its Roche lobe exactly, which is accurate to $\lesssim 0.1\%$.)

Verify that this indeed gives reasonable mass transfer rates if the condition for stable mass transfer is fulfilled.

Chapter 8

Conservative binary evolution

In the previous chapter we came to the conclusion that when mass transfer starts while the donor still has a radiative envelope, i.e. it first fills its Roche lobe on the main sequence or the Hertzsprung gap (case A or early case B), and if the initial mass ratio $M_1/M_2 \lesssim 4$, then mass transfer should occur on the donor's thermal timescale. Although this can imply quite high rates of mass transfer, the process itself is self-regulating and stable. Under such circumstances it is not unreasonable to make the assumption of conservative mass transfer (§ 7.2.1), because the matter that is transferred through the inner Lagrangian point does not have sufficient energy to escape from the companion's Roche lobe. In this chapter we therefore consider conservative binary evolution according to case A and case B.

Whether mass transfer really is conservative depends on the response of the companion star to accretion. This constitutes a still unsolved problems in the evolution of close binaries: how much mass and angular momentum are lost from a binary system during phases of stable Roche-lobe overflow, and how does this depend on the masses and orbital parameters of the binary. We will address this question in Sect. 8.3 of this chapter.

8.1 Case A evolution and the Algol systems

In short-period binaries evolving according to case A, the first phase of mass transfer can usually be divided into a rapid phase on the thermal timescale of the primary, followed by a slow phase on the much longer nuclear timescale. This is illustrated in Fig. 8.1, which shows the result of a detailed evolution calculation for the primary component in a binary with initial masses 10.0 and 8.9 $M_\odot$ and an initial period $P = 2.2$ d. The M-R diagram can be compared to Fig. 7.1 in the previous chapter. The rapid phase of mass transfer, starting at point B, continues until the primary has regained thermal equilibrium, i.e. when its equilibrium radius becomes smaller than its Roche radius (point C). By this time the primary has become the less massive star in the binary, in other words the mass ratio has been reversed. Further mass transfer is driven by expansion of the primary and takes place on the nuclear timescale, until the primary has reached the end of its main-sequence phase (point D).

For the same binary, Fig. 8.2 shows the evolution of both components. The binary is detached during phase A–B. During the rapid mass-transfer phase (B–C) both stars are out of thermal equilibrium: the primary is somewhat less luminous due to mass loss, while the secondary is somewhat more luminous as a result of accretion (see §8.3). At point C both stars have regained thermal equilibrium, and phase C–D is a long-lived phase of nuclear-timescale mass transfer. The secondary has a luminosity and radius appropriate for a MS star of its increased mass, but the now less massive primary is over-luminous for its mass, and has a larger radius than the secondary.

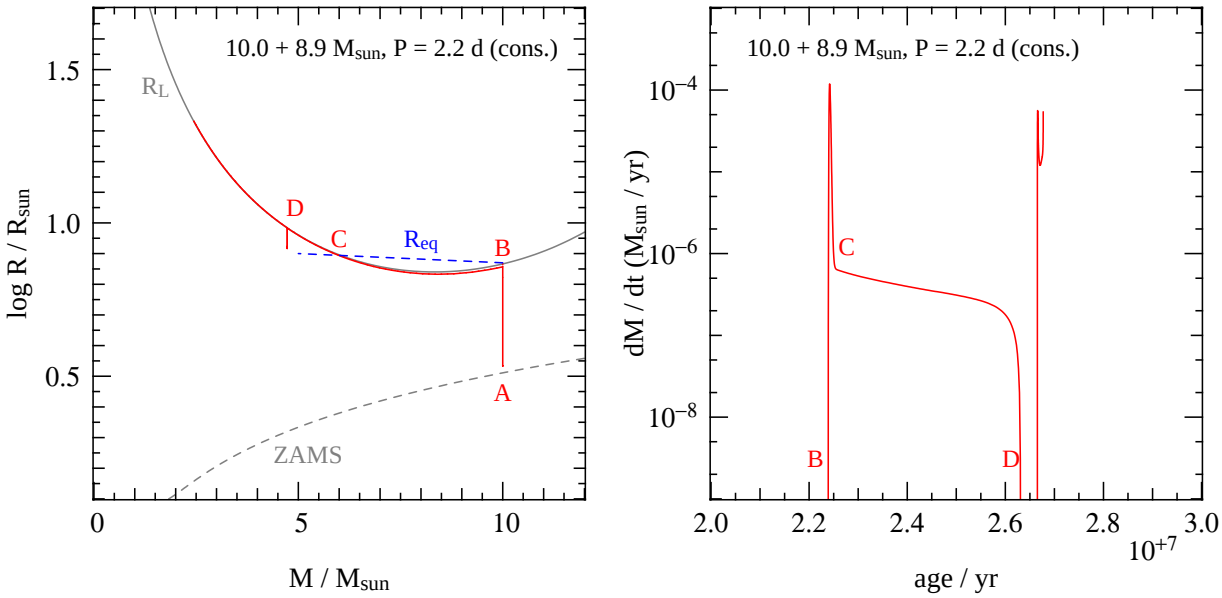

Figure 8.1. Mass-radius diagram of the primary star in a massive binary with initial parameters 10.0 + 8.9 $M_\odot$, P = 2.2 d, with metallicity Z = 0.004. The right diagram shows the corresponding mass transfer rate as a function of time. The primary expands during its main-sequence evolution from point A to point B, when it fills its Roche lobe. The dashed line indicates the equilibrium radius, which is larger than the Roche radius between B and C. This corresponds to a phase of rapid, thermal-timescale mass transfer. At C the primary regains thermal equilibrium, and further mass transfer (C-D) is driven by expansion and takes place on the nuclear (MS) timescale. Point D corresponds to the end of the MS phase of the primary, when it detaches from its Roche lobe for a short time. During H-shell burning the primary re-expands, giving rise to further mass transfer past point D (on the much faster expansion timescale associated with crossing the Hertzsprung gap).

Table 8.1. Some observed Algol-type binaries. Masses, radii and luminosities are given in solar units.

name	spectra	P (d)	M_1	M_2	R_1	R_2	$\log L_1$	$\log L_2$
V Pup	B2 + B1V	1.45	9	17	5.3	6.3	3.85	4.20
TT Aur	B6 + B3	1.33	5.4	8.1	4.2	3.9	3.21	3.71
U Her	B8-9 + B2V	2.05	2.9	7.6	4.4	5.8	2.49	3.68
Z Vul	A2III + B3V	2.45	2.3	5.4	4.5	4.7	2.07	3.30
U CrB	G0III + B5.5V	3.45	1.46	4.98	4.94	2.73	1.43	2.51
β Per (Algol)	G8III + B8V	2.87	0.8	3.7	3.5	2.9	0.65	2.27
V356 Sgr	A2III + B4V	8.90	4.7	12.1	14	6		

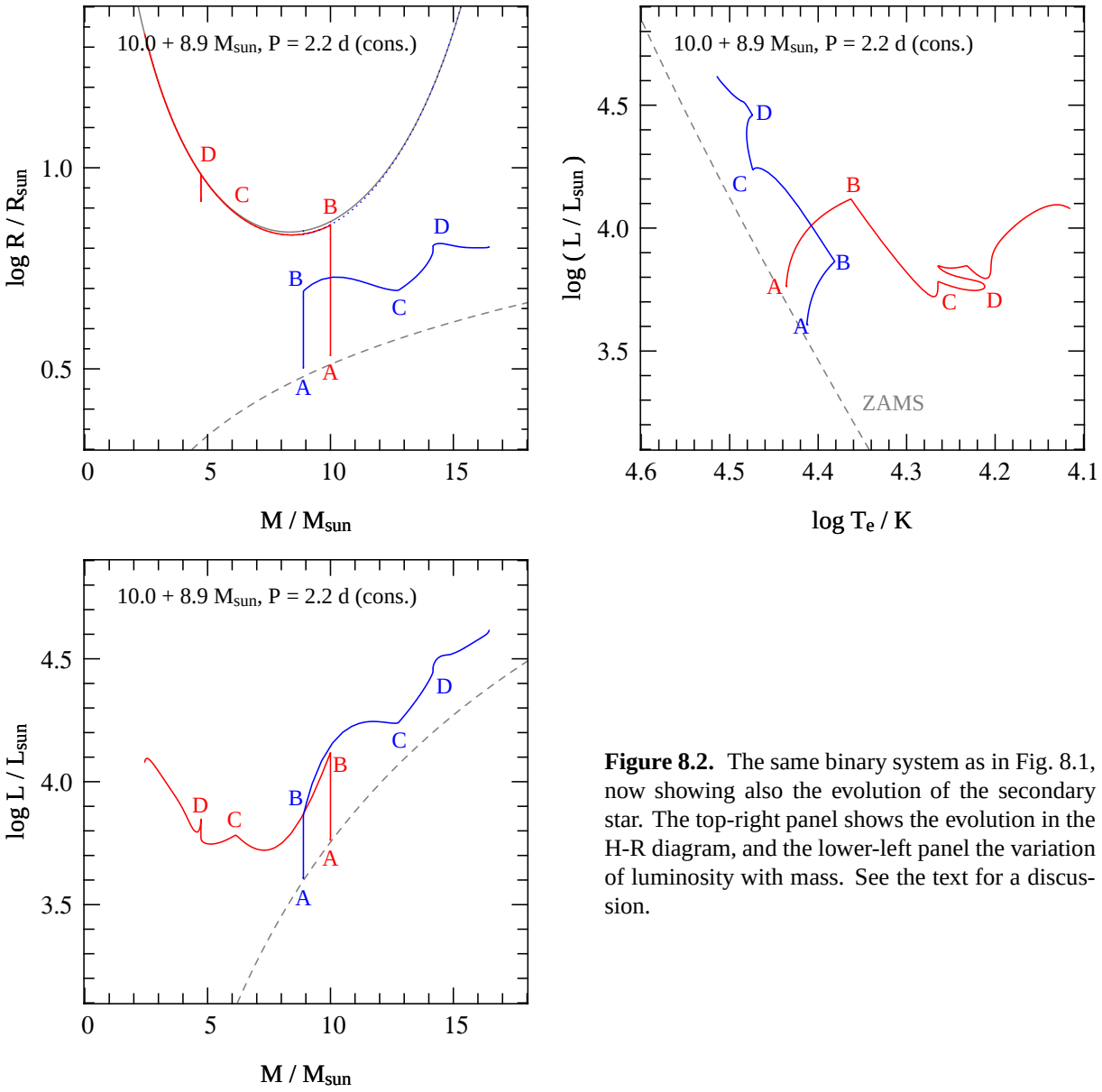

Figure 8.2. The same binary system as in Fig. 8.1, now showing also the evolution of the secondary star. The top-right panel shows the evolution in the H-R diagram, and the lower-left panel the variation of luminosity with mass. See the text for a discussion.

These properties are typical of many observed semi-detached binaries, so-called Algol-type binaries. Table 8.1 lists observed properties of several Algol-type systems. The primary (*1) is now filling its Roche lobe and is interpreted as the originally most massive star. The secondary (*2) is currently the more massive and more luminous star, but is often smaller in radius than the primary. Many such binaries are known, which is in accordance with the fact that the semi-detached phase of slow mass transfer lasts for the remaining main-sequence lifetime of the primary. The first group of six systems in Table 8.1 are interpreted as undergoing slow case A mass transfer. The last system is an example of a group of rarer, wider semi-detached systems that may be undergoing case B mass transfer (see § 8.2).

Nelson & Eggleton (2001) computed a large grid of conservative case A evolution models, covering the entire parameter space in masses and orbital periods. They compared their models to observed Algol binaries. This paper provides interesting background reading.

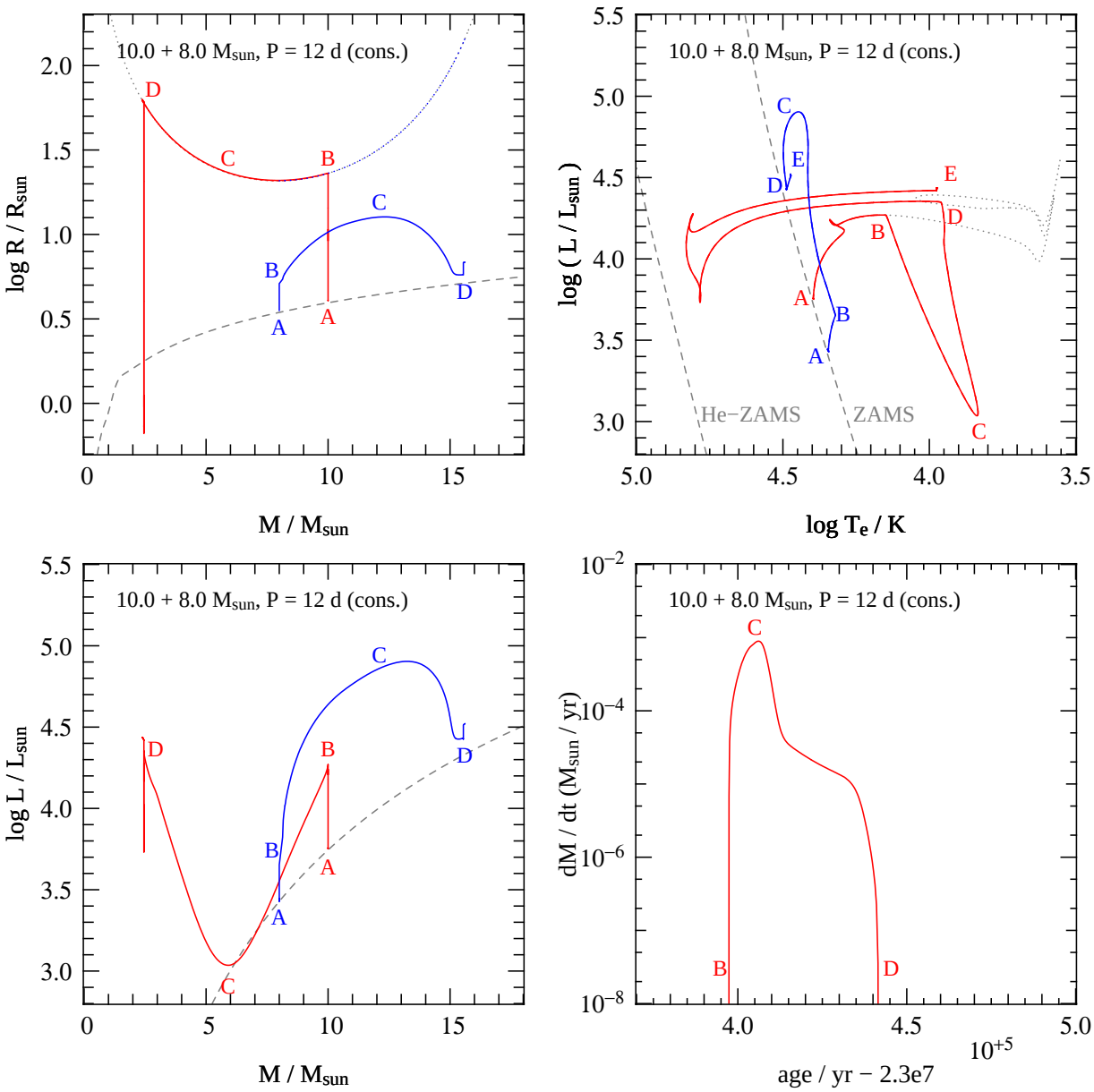

Figure 8.3. Conservative evolution of a binary of 10.0 + 8.0 $M_\odot$, P = 12 d, undergoing case B mass transfer. Panels are similar to those in Fig 8.2, with the bottom-right panel showing the mass transfer rate as a function of time. Note the expanded scale: the entire mass-transfer phase (B-D) lasts < 2% of the preceding MS lifetime. Point C corresponds to the maximum mass-transfer rate, coinciding with the minimum in the primary's luminosity and the maximum in the secondary's luminosity.

8.2 Case B evolution

Early case B mass transfer in intermediate-mass and massive binaries, with periods ranging from a few days to ~100 days, depending on the primary mass, is in many respects similar to case A. Since the donor's envelope is radiative mass transfer starts with a rapid, thermal-timescale phase during which the mass ratio is reversed. An important difference is that since the primary is more extended and therefore has a shorter thermal timescale (§ 6.2.2) compared to case A, the mass transfer rates during the rapid

Table 8.2. Some observed post-RLOF binaries. Masses and radii are given in solar units.

name	spectra	P (d)	M_1	M_2	R_1	R_2
CQ Cep	WN7 + O6	1.64	24	30	8.8	7.9
V398 Car	WN4 + O4-6	8.26	19	37		
GP Cep	WN6/WC + O3-6	6.69	15	27		
CV Ser	WC8 + O8-9	29.7	13	27		
V444 Cyg	WN5 + O6	4.21	9.3	28	2.9	8.5
ϕ Per	HeI em + B1IIIe	127	1.15	9.3	1.3:	5.5–8

phase are correspondingly higher. Furthermore the primary is itself in a rapid phase of evolution: while crossing the Hertzsprung gap it is out of thermal equilibrium and expands on the timescale at which its core contracts. As a consequence, after mass-ratio reversal mass transfer continues on the expansion timescale of the primary, only slightly slower than the thermal timescale. Therefore there is no 'slow' phase of mass transfer as in case A binaries. Mass transfer continues at a fairly high rate until most of the envelope has been transferred, as illustrated in Fig. 8.3. The evolution track describes a loop in the H-R diagram during the mass transfer phase, points B-D, with the maximum transfer rate coinciding with the minimum in luminosity of the primary at point C. The decrease in luminosity during mass transfer is caused by the strong thermal disequilibrium of the primary: as described in § 7.3 a radiative donor star shrinks in response to mass loss and has to re-expand to regain thermal equilibrium. This requires the absorption of gravitational energy, so that the surface luminosity during thermal-timescale mass transfer is (much) smaller than the nuclear luminosity provided by the H-burning shell.

When helium is ignited in the core (pomt D) mass transfer stops: the primary contracts and detaches from its Roche lobe. This happens when the primary is almost reduced to its bare helium core, with only a thin H-rich layer. The primary moves to a position close to the helium main-sequence in the H-R diagram. From single-star evolution models of intermediate-mass and massive stars, the mass of the helium core after the main sequence (when the star crosses the Hertzsprung gap) is well approximated by

$$M_{\rm core}/M_\odot = 0.10\,(M_{\rm i}/M_\odot)^{1.4}, \tag{8.1}$$

where $M_{\rm i}$ is the initial mass. If we make the assumption of conservative mass transfer, we can use this relation to either (1) predict the outcome of case B mass transfer, or (2) trace back the evolution of an observed binary that we believe to have undergone case B mass transfer.

Since the mass-transfer phase in case B binaries is very short compared to case A binaries, observational counterparts are rare. Indeed the vast majority of observed Algol-type binaries have short periods, $P < 10$ d. One likely example of a binary currently undergoing case B mass transfer is β Lyrae which we encountered in Exercise 7.2. On the other hand, the remnants of case B mass transfer are in a long-lived phase of evolution: these are binaries consisting of the almost bare helium-burning core of the primary and a more massive main-sequence star. Conservative mass transfer will have widened their orbits significantly. Observed counterparts of this evolution phase among massive systems are the WR+O binaries, consisting of a Wolf-Rayet star and a massive O star. Some examples are given in Table 8.2. Among intermediate-mass binaries on the other hand, not many counterparts are known. This is probably a selection effect: the He star is much hotter and less luminous than its companion, so it will be optically much fainter. Furthermore its low mass and the wide orbit after conservative mass transfer imply that the orbital velocity of the main-sequence star is undetectably small. The best candidate for this phase of evolution is the binary ϕ Persei: a binary with $P_{\rm orb} = 127$ d consisting of a B1e main sequence star and a He emission-line object, presumably a naked He-burning star (Gies et al., 1998, see Table 8.2).

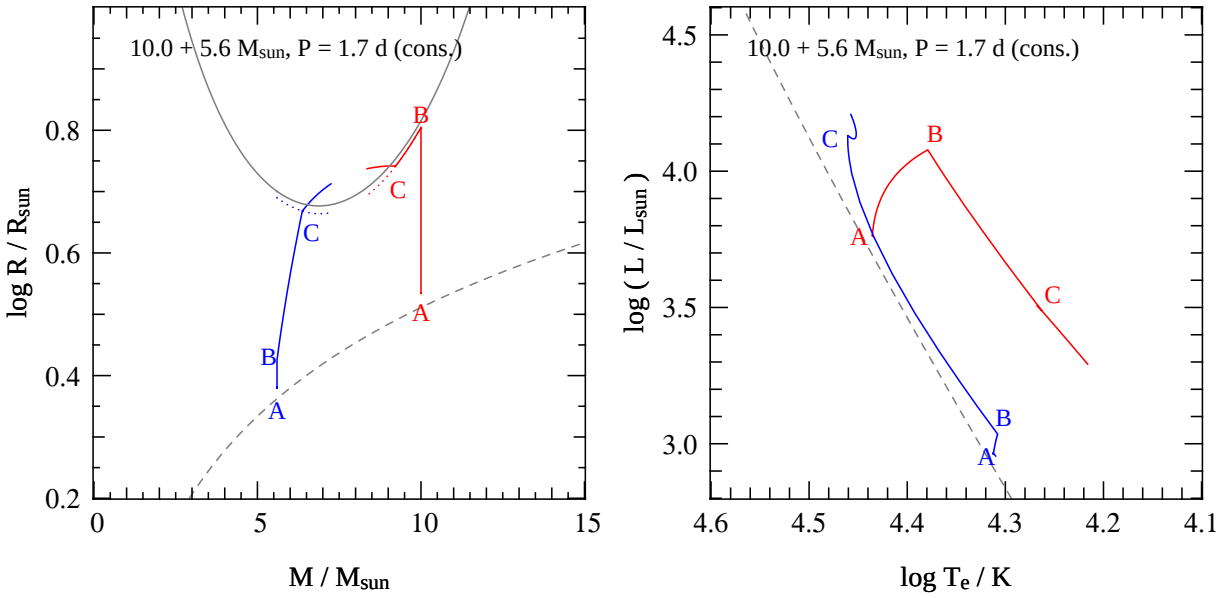

Figure 8.4. Similar to Fig 8.2, but for a binary with a more extreme initial mass ratio. The large difference in thermal timescales between the primary and secondary causes the secondary to become highly over-luminous and expand in response to accretion. As a result the secondary fills its Roche lobe during rapid mass transfer, after only a small amount of accretion, and a contact binary is formed at point C.

8.3 The response of the mass gainer

The mass transfer stream from the donor will follow a more-or-less ballistic orbit, reaching a minimum distance $d_{\rm min}$ from the center of mass of the companion which scales with the orbital separation. The stream hits the accreting star directly if $R_{\rm a} > d_{\rm min}$, otherwise it continues in its orbit and collides with itself, forming an accretion disk around the companion. This latter possibility occurs in relatively wide orbits, compared to the companion's radius. As a consequence not only mass but also angular momentum is transferred to the companion. Accretion onto the companion star therefore has three important consequences for its structure and evolution[1]:

Thermal readjustment and expansion

The secondary star has to adjust its structure to the added mass. The main effect of accretion is the compression of underlying layers which releases gravitational energy. If this energy release is larger than the luminosity of the star it will be brought out of thermal equilibrium. This is the case if accretion takes place on a timescale shorter than the accretor's Kelvin-Helmholtz timescale. One may then expect the reverse of the effect of rapid mass loss on the donor star (§ 7.3): accretion onto a star with a convective envelope makes it shrink, while accretion onto a star with a radiative envelope causes it to expand. This is indeed borne out by detailed calculations.

During the first mass transfer phase the thermal timescale of the secondary is longer than that of the donor, so that the accretor will be brought out of thermal equilibrium. This makes it brighter than the main-sequence luminosity appropriate for its mass, and for sufficiently high accretion rates, also causes

[1]One should also consider the kinetic energy of the stream but this is probably dissipated locally and radiated away, either in the accretion disk and its boundary layer, or in a 'hot spot' where the stream hits the stellar surface, and therefore does not add to the energy budget of the accreting star.

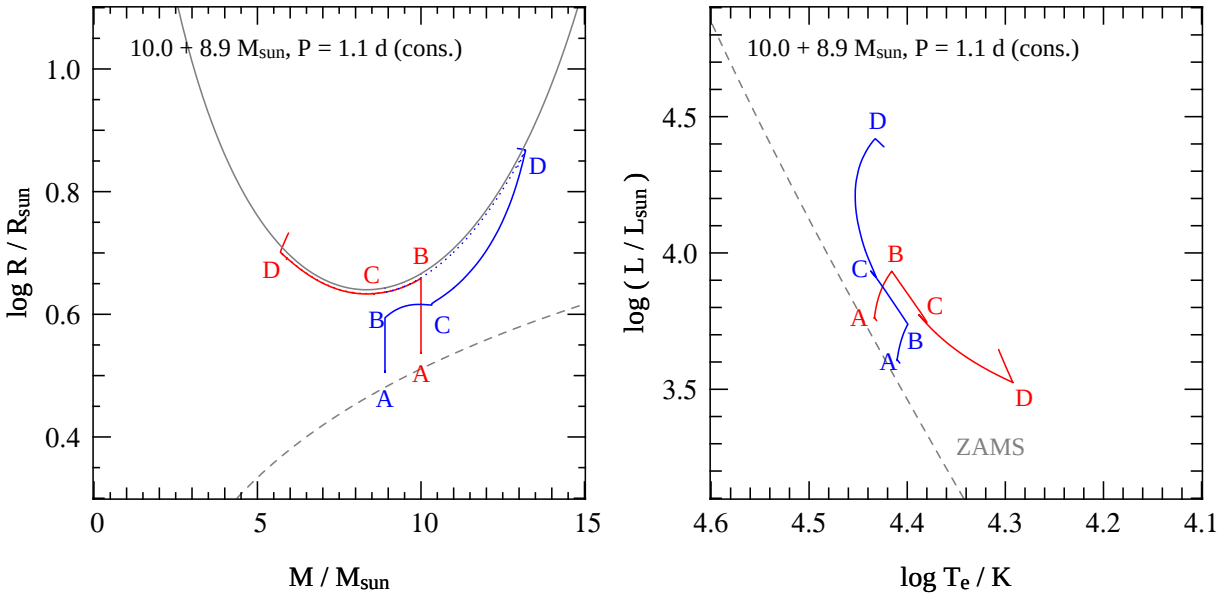

Figure 8.5. Similar to Fig 8.2, but for a binary with a smaller orbital period. During rapid mass transfer (BC) the secondary remains close to thermal equilibrium, but during the subsequent slow mass transfer (C-D) its evolution speeds up and eventually overtakes that of the primary. As a result a contact binary is formed at point D.

substantial expansion of the star over its main-sequence radius (see Fig. 8.3, point C on the evolution track of the secondary). As a consequence the secondary may fill its own Roche lobe and a contact binary can be formed. An example of this is given in Fig. 8.4.

Spin-up of the accreting star

The matter that is transferred to the secondary carries a significant amount of angular momentum, especially if it passes through an accretion disc. This can bring the secondary to break-up rotation after accreting only about 10 % of its original mass (Packet, 1981). The secondary then has to get rid of some, or most, of its angular momentum before further accretion can take place. Hence this 'angular momentum catastrophe' potentially limits the amount of accretion much more than the effect of expansion discussed above. Tidal interaction with the companion can transfer spin angular momentum back into the orbit, thus preventing critical rotation, but only in very close binaries with periods less than a few days. Another way by which the accreting star may get rid of its angular momentum is by mass loss. In massive binaries at least, the (normally weak) stellar wind may be enhanced enormously when the star is rotating very close to critical; this enhanced wind takes away the excess angular momentum. This process necessarily leads to non-conservative mass transfer, and a small value of the mass transfer efficiency parameter β (discussed in §7.2.2).

Despite these theoretical considerations, it appears that close-to-conservative mass transfer *does* occur in practice even in systems that are too wide for tidal interaction to be important, and of too low mass for stellar winds to be significant. A case in point is the Be-star binary ϕ Per discussed above, whose wide orbit and small mass ratio are indicative of conservative mass transfer. The secondary component is a rapidly rotating Be star, presumably as a result of spin-up by mass transfer. The same process is responsible for the formation of the Be stars seen as companions in many high-mass X-ray binaries. If the component masses in ϕ Per had been a factor ~2 higher, it would have been the perfect progenitor system of such a Be/X-ray binary.

Rejuvenation

If mass transfer is indeed (close to) conservative then the mass of the secondary is increased significantly. This has two effects on its further evolution. First, the added mass causes its convective core to grow in mass, mixing in fresh fuel from outer layers into the nuclear-burning zone in the center. This process is called rejuvenation, since it has the effect of extending the main-sequence lifetime of the secondary.[2] This can be seen in Fig 8.3 where after mass transfer (point D) the secondary is closer to the ZAMS than at the start (point B). The rejuvenation effect is counteracted, however, by the fact that its nuclear timescale (which scales approximately with $M^{-2.8}$, § 6.2.2) becomes much shorter. The combined result is that the secondary can overtake the evolution of the primary under some circumstances. An example of this is given in Fig. 8.5.

8.3.1 Formation of contact binaries

A number of studies have investigated for which binary parameters the secondary can evolve into contact (Pols, 1994; Nelson & Eggleton, 2001; Wellstein et al., 2001). In these binary evolution calculations the spin-up of the secondary was neglected. The results indicate that contact arises in three different circumstances:

1. During rapid (thermal timescale) RLOF, either in case A or early case B. This occurs for $M_1/M_2 > q_{\rm cr}$, where $q_{\rm cr}$ is in the range $1-2$ depending on primary mass. In this case the thermal timescale of the accretor is much longer than the accretion timescale, so that it swells up quickly and fills its Roche lobe after accreting only a small amount of mass (e.g. Fig. 8.4).

2. During the slow (nuclear timescale) phase RLOF in case A after the mass ratio is reversed. For very short $P_{\rm orb}$ the nuclear evolution of the secondary can then overtake that of the primary (e.g. Fig. 8.5). The ensuing contact stage may be quite long-lived given that massive contact binaries are not uncommon, but the evolution of such systems is not well understood.

3. During the late phase of RLOF in case B for fairly long periods, when $\dot{M}$ accelerates as the envelope of the donor becomes partly convective. In this case, a contact binary is formed after substantial mass accretion has already taken place.

Based on the above, regions in parameter space (q_0 and P_0) where contact is avoided can be identified. Examples of this can be found in the papers cited above.

Neglecting other effects, one might expect conservative mass transfer in those systems that avoid contact altogether, and up to the point where contact is reached in the other cases. However, the further evolution of contact binaries is highly uncertain, and how much mass and angular momentum these systems lose are still open questions. It seems likely that a case A contact binary must eventually merge to a single star, while in a case B situation the contact binary may quickly evolve into a common-envelope configuration (§ 10.2).

Exercises

8.1 Consider the binary depicted in Fig. 8.1. Verify that the rapid mass-transfer phase (B–C) indeed takes place on the thermal timescale of the donor, and that the slow phase (C–D) takes place on the nuclear timescale of the donor. Assume typical values for a $10\,M_\odot$ main-sequence star.

[2] Not all detailed evolution models of accreting stars show such rejuvenation, it depends on the uncertain mixing efficiency in semi-convective layers.

8.2 We have seen that for case B mass transfer in intermediate-mass or massive binaries, almost the entire envelope of the donor star is transferred and the remnant is the almost bare helium core of the donor. For a binary system with masses $4 + 3\,M_\odot$, see Exercise 6.3, calculate the masses of the components after conservative case B mass transfer. Subsequently calculate the range of final orbital periods after conservative case B mass transfer, taking into account for which systems you may reasonably expect the conservative assumption to hold.

8.3 Compare the outcome of case B mass transfer for a primary mass of $4\,M_\odot$ (previous exercise) with that of $10\,M_\odot$ and $40\,M_\odot$, assuming the same initial mass ratio of 0.75, in terms of (a) the final mass ratio and (b) the ratio of final to initial orbital period.

8.4 Assuming the He-star + Be-star system ϕ Persei (see Table 8.2) formed by conservative case B mass transfer, calculate the initial masses and orbital period of the binary. Is this consistent with the case B assumption?

Chapter 9

Observed binaries with compact objects

This chapter provides an overview of observed types of binaries in which one or both stars are compact objects (white dwarfs, neutron stars or black holes). In many of these systems an important energy source is accretion onto the compact object.

9.1 Accretion power

When mass falls on an object of mass M and with radius R, at a rate $\dot{M}$, a luminosity $L_{\rm acc}$ may be produced:

$$L_{\rm acc} = \frac{GM\dot{M}}{R} \tag{9.1}$$

The smaller the radius, the more energy can be released. For a white dwarf with $M \approx 0.7\,M_\odot$ and $R \approx 0.01\,R_\odot$, this yields $L_{\rm acc} \approx 1.5 \times 10^{-4}\dot{M}c^2$. For a neutron star with $M \approx 1.4\,M_\odot$ and $R \approx 10\,$km, we find $L_{\rm acc} \approx 0.2\dot{M}c^2$ and for a black hole with Scwarzschild radius $R \sim 2GM/c^2$ we find $L_{\rm acc} \sim 0.5\dot{M}c^2$, i.e. in the ideal case a sizable fraction of the rest mass may be released as energy. This accretion process is thus potentially much more efficient than nuclear fusion.

However, the accretion luminosity should not be able to exceed the Eddington luminosity,

$$L_{\rm acc} \leq L_{\rm Edd} = \frac{4\pi cGM}{\kappa} \tag{9.2}$$

where κ is the opacity, which may be taken as the electron scattering opacity, $\kappa_{\rm es} = 0.2(1 + X)\,{\rm cm}^2/{\rm g}$ for a hydrogen mass fraction X. Thus the compact accreting star may not be able to accrete more than a fraction of the mass that is transferred onto it by its companion. By equating $L_{\rm acc}$ to $L_{\rm Edd}$ we obtain the maximum accretion rate,

$$\dot{M}_{\rm Edd} = \frac{4\pi cR}{\kappa} \tag{9.3}$$

The remainder of the mass may be lost from the binary system, in the form of a wind or jets blown from the vicinity of the compact star, or it may accumulate in the accretor's Roche lobe or in a common envelope around the system. For a white dwarf with $R \approx 0.01\,R_\odot$ accreting hydrogen-rich gas ($X = 0.7$) we find $\dot{M}_{\rm Edd} \approx 1.2 \times 10^{-5}\,M_\odot/{\rm yr}$, and for a neutron star with $R \approx 10\,$km, $\dot{M}_{\rm Edd} \approx 1.7 \times 10^{-8}\,M_\odot/{\rm yr}$.

9.2 White dwarf binaries

Among main-sequence binaries with unseen companions, a sizable fraction will contain a white dwarf that has cooled beyond detection. Here we discuss only those systems in which the white dwarf is

Table 9.1. Some close white-dwarf binaries. Masses and radii are given in solar units. If no eccentricity is given the orbit is circular. Mass values in *italics* indicate the measured mass function, rather than the mass.

name	spectra	P (d)	e	M_1	M_2	R_1	R_2
close binaries inside planetary nebulae							
KV Vel	sdO + CIIIe	0.357		0.63	0.23	0.16	0.40
UU Sge	sdO + M?	0.465		0.63	0.29	0.33	0.54
V477 Lyr	sdO + M?	0.472		0.51	0.15	0.17	0.46
BE UMa	sdO + M?	2.29		0.7:	0.36:	0.08:	0.7:
V651 Mon	sdO + A5Vm:	16.0	0.07:		*0.0073*		
detached white dwarf-main sequence binaries							
HR Cam	WD + M	0.103		0.41	0.10	0.018	0.125
13471-128	WD + M3.5/4	0.151		0.78	0.43	0.011	0.42
NN Ser	WD + M5-6	0.130		0.57	0.12	0.019	0.17
CC Cet	WDA2 + M4.5e	0.284		0.39	0.18		0.21
GK Vir	WDAO + M3-5V	0.344		0.51	0.10		0.15
V471 Tau	WD + K2V	0.521		0.84	0.93	0.011	0.96
Feige 24	WD + M1.5V	4.23		0.47	0.30	0.032	
double white dwarf binaries							
0957-666	WDA + WDA	0.061		0.32	0.37		
1101+364	WDA3 + WDA	0.145		0.33	0.29		
1704+481a	WDA4 + WD	0.145		0.56	0.39		
HE 1414-0848	WD + WD	0.518		0.55	0.71		
1399+144	WD + WD	2.209		0.44	0.44		

observed directly, or its presence is revealed by current or past interaction with its companion. Binaries consisting of a white dwarf plus a normal star can be divided into systems with close orbits ($P \lesssim 10$ d) and those with relatively wide orbits ($P \gtrsim 100$ d).

9.2.1 Close detached white-dwarf binaries

Several white dwarfs have been detected in a close detached orbit ($P \lesssim 10$ d) around a low-mass main-sequence star. Some examples are given in Table 9.1. In these systems the orbits are much smaller than the size of the red-giant progenitor of the white dwarf, and their formation requires strong mass and angular momentum loss in the form of a common envelope phase and spiral-in (to be discussed in § 10.2).

Closely related are so-called double cores of planetary nebulae, in which the hot nucleus of the nebula which will later cool into a white dwarf is accompanied by a low-mass star in a close orbit. About 5 to 10 per cent of all planetary nebulae have such double cores. In these systems the nebula is probably the ejected common envelope that formed the close binary. These detached binaries may evolve, by means of either angular momentum loss from the orbit (to be discussed in § 11.3) or nuclear expansion of the main-sequence star, into one of the two types of semi-detached, interacting binaries discussed in § 9.2.2.

Double white dwarfs Many short period binaries consisting of two white dwarfs have been discovered in recent years, see Table 9.1 for a few examples. Their orbital periods range from $P \sim 0.06$–30 d. In most cases the masses of the white dwarfs are low, $\lesssim 0.45\,M_\odot$, which means that they must be composed of helium rather than carbon and oxygen. The masses of the two white dwarfs are often rather similar,

Table 9.2. Some cataclysmic variables and supersoft X-ray sources. Masses and radii are given in solar units. Types: CN - classical nova; DN - dwarf nova; MP - magnetic polar; IP - intermediate polar; UCB - ultra-compact binary; SSX - supersoft X-ray source.

name	spectra	type	P (d)	M_1	M_2	R_1	R_2
AM CVn	He em	UCB	0.012		0.04:		
OY Car	sdBe + M7-8	DN	0.063	0.685	0.07		0.127
Z Cha	sdBe + M5.5V	DN	0.075	0.84	0.125		0.17
AM Her	sdBe + M4V	MP	0.129	0.44	0.29		0.33
U Gem	sdBe + M4V	DN	0.177	1.26	0.57		0.51
DQ Her	sdBe + M3V	CN, IP	0.194	0.60	0.40		0.49
BT Mon	sdBe + G8V	CN	0.334	1.04	0.87		0.89
GK Per	sdBe + K1IV	CN, DN	2.00	0.9:	0.5:		2.5:
V Sge	WN: + B8:	SSX	0.514	0.9:	3.3:		2.1
U Sco	sdBe + F8V	SSX	1.23	1.55:	0.88		2.1

which provides important clues for their formation. The closest systems among them are expected to merge within a Hubble time due to angular momentum loss by gravitational radiation.

9.2.2 Cataclysmic variables and related systems

Cataclysmic variables The name of this group derives from their outbursting nature, they comprise the *classical novae* and related systems, see Table 9.2. They consist of a low-mass main-sequence star and a white dwarf, the MS star is filling its Roche lobe and transferring mass to the WD via an accretion disk. Orbital periods are typically $0.05\,\mathrm{d} \lesssim P \lesssim 0.5\,\mathrm{d}$, with a few exceptions. Inbetween outbursts, the accretion disk is often the main source of light in the system. The white dwarf is more massive than its companion, $q = M_{\rm MS}/M_{\rm WD} \lesssim 0.7$ so that Roche-lobe overflow is stable and occurs at a low rate ($\dot{M} \sim 10^{-11}$–$10^{-9}\,M_\odot$/yr). The low accretion rate leads to hydrogen piling up on the surface of the white dwarf, until it ignites in a flash when the pressure and temperature at the bottom of the accreted layer are high enough for fusion. The resulting thermonuclear runaway leads to the observed nova outbursts during which the visual luminosity increases by a factor 10^4–10^6.

Probably all cataclysmic variables undergo nova outbursts, but only in a subset of them have they been observed. This is consistent with the expected time between thermonuclear flashes, $\gtrsim 10^4$ years. Many other CVs, known as *dwarf novae*, show outbursts of a different kind, milder in nature (up to a factor 10^2 in luminosity) and occurring every few weeks. These are probaly the result of an instability in the accretion disk, which builds up until the viscosity suddenly increases and the accumulated mass is rapidly dumped onto the white dwarf. In other systems, known as *polars*, the white dwarf is highly magnetized and dominates the accretion flow, either completely (magnetic polars, in which the accretion disk is absent and the white dwarf rotation is locked with the orbit) or partly (intermediate polars, which have small accretion disks truncated on the inside by the white-dwarf magnetosphere).

Supersoft X-ray sources The sensitivity of ROSAT to photons with energies $\lesssim 500\,\mathrm{eV}$ has led to the discovery of a new class of X-ray sources that emits only at these low energies. Various types of objects could give rise to such very soft X-ray emission. The most luminous persistent sources, with $L \sim 10^{36-38}$ erg/s and blackbody temperatures of several times 10^5 K, are white dwarfs undergoing steady nuclear burning of hydrogen on their surfaces. Theoretical accretion models show that this happens if a WD accretes at a steady rate of $1\text{–}2 \times 10^{-7}\,M_\odot$/yr. This is typically what is expected for thermal-

Table 9.3. Some symbiotic and barium-star binaries. The last column gives the mass function of the giant (secondary) component; radial velocity variations of the white dwarf are generally not measured.

name	spectra	P (d)	e	$f(M_2)$
	symbiotic binaries			
T CrB	Be + M4III	227.7	0	0.32
AG Dra	sdOe + K3pII	549	0.13	0.008
BD Cam	WD + M3/S5	597	0.09	0.037
	barium star systems			
HD 77247	? + G7IIBa	80.53	0.09	0.0050
105 Her	? + K3IIBa	486	0.36	0.135
ξ^1 Cyg	WD + G7IIIBa	1642	0	0.035
ζ Cap	WD + G5IbBa	2380	0.28	0.0042
ζ Cyg	WD + G8IIIBa	6489	0.22	0.0227

timescale mass transfer from a main-sequence or subgiant donor of 1.3–2.5 $M_\odot$ to a less massive white dwarf. Their orbital periods typically range from 0.2 to 4 d, making SSXs the higher-mass analogues of CVs. The steady accretion rate may bring the white dwarf over the Chandrasekhar limit, and these systems are currently considered as the most likely progenitors of Type Ia supernovae. (In contrast, in CVs the nova outbursts eject most or all of the previously accreted mass so that the white dwarf mass does not grow.)

9.2.3 Symbiotic binaries and related systems

Symbiotic stars show the combined spectrum of a cool giant superimposed with emission lines of hydrogen and helium. The emission spectrum comes from a hot white dwarf that accretes matter from its red giant or AGB companion, either from the strong stellar wind of the giant or in some cases by Roche-lobe overflow. The accretion (at rates up to 10^{-7} $M_\odot$/yr) heats the white dwarf so that it competes in luminosity with the red giant (100–1000 $L_\odot$) and becomes visible. The orbital periods of symbiotic binaries range from $P \sim 10^2$–10^4 days. Several symbiotics show nova outbursts, often recurrent in nature (symbiotic novae) and some are also observed as supersoft X-ray sources. Hence the classes of symbiotic binaries and cataclysmic variables partly overlap.

Related to symbiotic binaries in their evolutionary history, but different in appearance, are the barium and CH stars. They are red giants or subgiants in binaries with similar periods ($P \sim 10^2$–10^4 d) but the white dwarf is usually not directly observed. The presence of a white dwarf is inferred, apart from the radial velocity variations, from the abundance anomalies in the spectrum of the (sub)giant which is enhanced in carbon and heavy s-process elements, in particular barium. These elements were produced by the progenitor of the white dwarf while it was an AGB star and have been transferred to the lower-mass main-sequence companion, now seen as a giant.

9.3 Neutron star and black hole binaries

Binaries containing a neutron star or a black hole can be observed as strong sources of X-rays as a result of accretion onto the compact object (eq. 9.1) in which case they are known as X-ray binaries. In the absence of accretion, a neutron star (but not a black hole) in a binary can be observed as a binary radio pulsar (§ 9.3.4).

Investigation of the properties of the brightest X-ray sources showed that they can be divided in two clearly separate types (Figure 9.2). Some sources emit their X-rays partially pulsed, others only show irregular variations. Many systems in the latter category occasionally show sudden surges in the X-ray flux: the X-ray bursts.

9.3.1 X-ray pulsars: high-mass X-ray binaries

The model for X-ray pulsars is that they are neutron stars with a strong dipolar magnetic field, which focusses the accreting matter to the magnetic poles, where it is stopped and emits X-rays. As the poles rotate in and out of view, we observe pulses of X-rays. The spectra of X-ray pulsars are hard, and photons are detected to energies above 50 keV. Signs of the magnetic fields are thought to have been detected in the form of cyclotron absorption lines in the X-ray spectra.

Optical identification was not easy in the early days, as the X-ray pulsars are located in the Galactic Plane, which means that the relatively large positional error boxes are crowded with stars. Nonetheless, many X-ray pulsars were succesfully identified, and their optical counterparts almost invariably are massive O or B stars. The X-ray pulse period varies due to the orbital motion of the neutron star around its companion; when the radial velocity curve of the O or B star can be measured as well, we have a double-lined spectroscopic binary. If in addition the neutron star is eclipsed by its companion, classical binary techniques can be employed to determine the masses of both stars. The neutron star masses cluster around 1.4 $M_\odot$, as expected from theory.

Some X-ray sources with an O or B companion star do not show pulses. The X-ray source in these may still be a neutron star. In some cases, however, which include Cyg X-1 and LMC X-3, the orbital velocity of the O or B supergiant indicates a mass for the compact star in excess of the maximum mass that is possible for a neutron star, and it is concluded that the compact star must be a black hole. The X-ray spectra of these black hole candidates contain more photons both at low energies (< 1 keV) and at high energies (up to > 100 keV) than the pulsar spectra.

Mass determinations are feasible in the systems with relatively short orbital periods, $P_{\rm orb} \lesssim 10$ d, in which the companion of the neutron star is an O or B supergiant. Many systems have rather longer orbital periods, up to more than a year. In these, the companion is usually a Be star, i.e. a rapidly rotating B star, and the X-ray emission is only detected occasionally. Taking selection effects against detection of

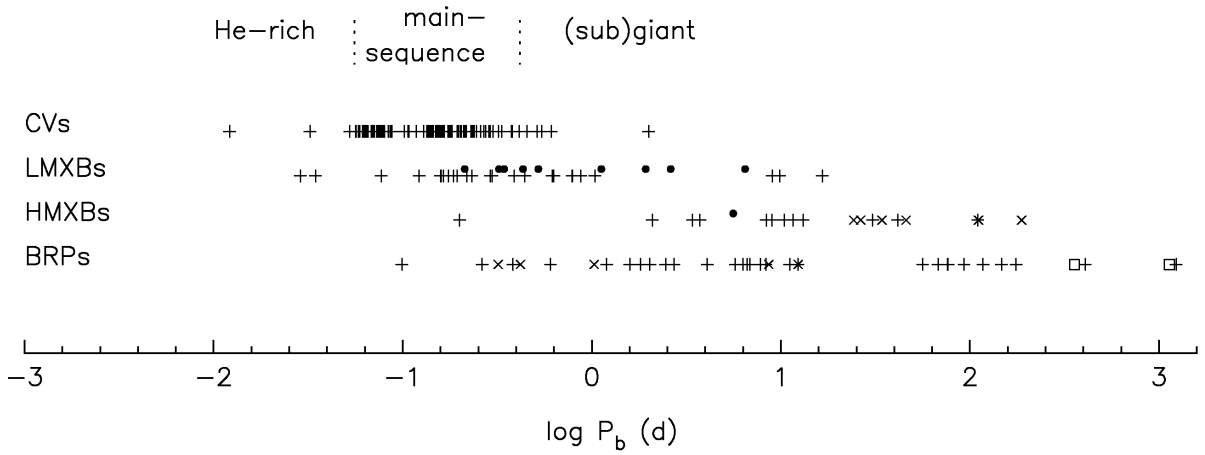

Figure 9.1. Orbital periods of cataclysmic variables, X-ray binaries and binary radio pulsars in our Galaxy. Each symbol indicates one system. For the X-ray binaries • indicates a system with a black hole, and × a Be donor star. For the binary radio pulsars + indicates a system with a low-mass white dwarf companion, × a system with a high-mass white dwarf or neutron star companion, and □ a main-sequence companion.

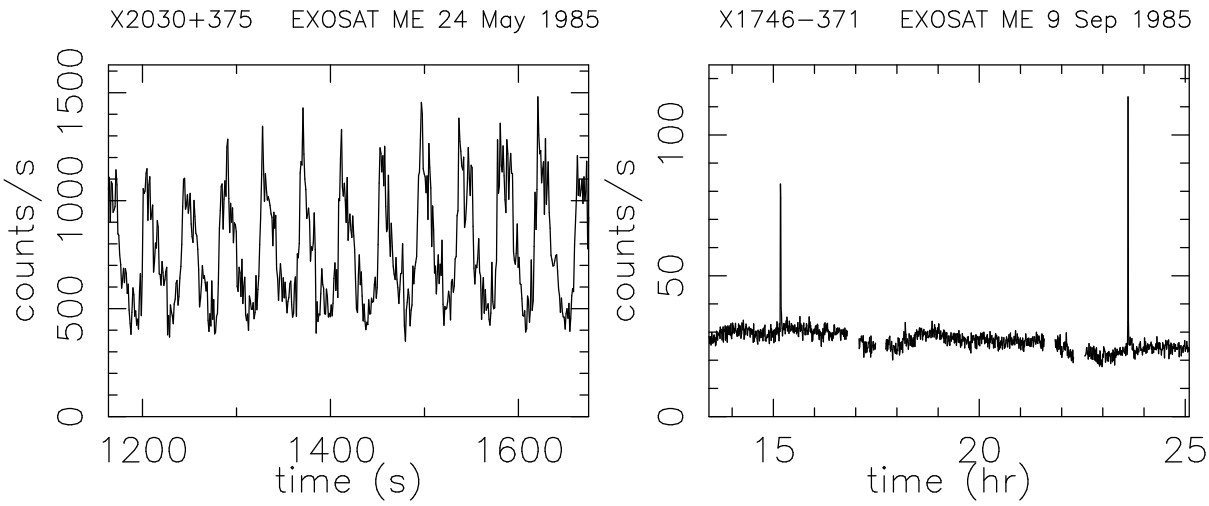

Figure 9.2. X-ray lightcurves, obtained with EXOSAT, of an X-ray pulsar, EXO 2030+375 (left), and of a burster, X1746-371, with two bursts visible (right).

such transient hard X-ray sources into account, we conclude that the Be-star + X-ray-pulsar binaries are in fact much more common (a few thousand in the Galaxy) than the supergiant + X-ray-pulsar systems (a dozen in the Galaxy). For both types of systems we find that the X-ray luminosity emitted near the neutron star is of the order of the optical luminosity of the O or B star.

The pulse periods of all X-ray pulsars vary, on time scales ranging from $P/\dot{P} \approx 100\,\mathrm{yr}$ to $10^6\mathrm{yr}$. These short time scales indicate that the moment of inertia, and hence the radius, of these objects are very small, in agreement with the theoretical estimates for neutron-star radii of $\sim 10\,\mathrm{km}$.

9.3.2 X-ray bursters: low-mass X-ray binaries

Soon after the discovery of the X-ray bursts, it was realized that these are caused by the sudden fusion into carbon of a helium layer on a neutron star, deposited there by the accretion of hydrogen which fuses immediately into helium. Thus, a burst is the neutron-star analogue of a nova outburst for a white dwarf. The X-ray spectra of the X-ray bursts have characteristic temperatures of $kT \lesssim 5\,\mathrm{keV}$. The steady X-ray spectrum of the luminous burst sources is soft; less luminous sources have power-law spectra. The spectra of sources of variable luminosity change accordingly.

Orbital periods for X-ray sources without pulses could be determined in larger numbers only after the launch of EXOSAT, whose wide orbit allowed four days of uninterrupted observing, and after the introduction of CCD photometry, which is capable of detecting small flux variations accurately. The orbital periods span the same range as those of the cataclysmic variables, which by analogy is taken to suggest that the companion to the neutron star is a low-mass star, close to the main sequence. These X-ray sources are therefore called low-mass X-ray binaries. Direct measurements of the properties of the donor star are hard to obtain, because the optical luminosity is dominated by reprocessing into the optical of X-rays that impinge on the accretion disk around the neutron star. The optical luminosity of these systems is much less than the X-ray luminosity, $L_{\mathrm{opt}} \lesssim 0.01 L_{\mathrm{x}}$, say. Even though the low-mass X-ray binaries often are well away from the Galactic Plane, with $|z| \approx 1\,\mathrm{kpc}$, their low visual brightness impedes easy optical identification.

The thick accretion disk also is responsible for the paucity of eclipsing low-mass X-ray binaries: when the inclination is high enough for the neutron star to be eclipsed by its companion, the probability is high that it is hidden altogether by the accretion disk.

Some low-mass X-ray binaries are transient sources. In these, the optical flux from the disk disap-

Table 9.4. Name, position, pulse period, X-ray luminosity, orbital period and eccentricity, and (for high-mass systems) the spectral type of the donor, for representative X-ray binaries. Binaries containing a black hole, and transients are indicated with B and T, respectively. For transients, the luminosity is the luminosity at outburst maximum. It should be noted that luminosities are uncertain due to uncertain distances for many sources.

name	position	$P_{\rm pulse}$ (s)		log $L_{\rm X}$ (erg/s)	P (d)	e	sp.type
high-mass X-ray binaries							
LMC X-4	0532 – 66	13.5		38.6	1.4	0.011	O7III
LMC X-3	0538 – 64	-	B	38.5	1.7	∼0	BIII-IV
Cen X-3	1119 – 60	4.8		37.9	2.1	0.0007	O6.5II
SMC X-1	0115 – 74	0.7		38.8	3.9	<0.0008	B0I
Cyg X-1	1956 + 35	-	B	37.3	5.6	∼0	O9.7I
Vela X-1	0900 – 40	283		36.8	9.0	0.092	B0.5I
LMC tran	0535 – 67	0.069		T 39.0	16.7	∼0.7	B2IV
V635 Cas	0115 + 63	3.6		T 36.9	24.3	0.34	Be
BQ Cam	0331 + 53	4.4		T 35.8	34.3	0.31	Be
GX301-2	1223 – 62	696		37.0	41.5	0.47	B1-1.5
V725 Tau	0535 + 26	104		T 37.3	111.0	0.3-0.4	Be
low-mass X-ray binaries							
KZ TrA	1627 – 67	7.7		36.8	0.029		
V1405 Aql	1916 – 05			36.9	0.035		
UY Vol	0748 – 68			T 37.0	0.159		
V4134 Sgr	1755 – 34			36.8	0.186		
V616 Mon	0620 – 00		B	T 38.3	0.323		
N Mus 1991	1124 – 68		B	T 37.6	0.427		
Cen X-4	1455 – 31			T 38.0	0.629		
Sco X-1	1617 – 16			37.5	0.787		
V404 Cyg	2023 + 33		B	T 38.4	6.500		
peculiar systems							
Her X-1	1656 + 35	1.2		36.8	1.7	< 0.0003	A9-B
Cyg X-2	2142 + 38			38.0	9.843		A9
Cyg X-3	2030 + 41			38.0	0.2		WN
Cir X-1	1516 – 57			T 38.9	16.6		
SS433	1909 + 05			35.8	13.2		
bursting pulsar	1744 – 28	0.467		T 38.9	11.8		accretion bursts
bursting pulsar	1808 – 36	0.0025		T 36.8	0.084		thermonuclear bursts

pears with the X-ray flux, and the companion becomes optically detectable. The radial velocity curve of the companion can then be measured. The companions in transients indeed appear to be low-mass stars, i.e. with spectral type G or K. In an increasing number of such transients the mass function indicates that the compact accreting star is a black hole. The X-ray spectra of transients with a black hole are remarkably similar to those of transients with a neutron star; the difference being that at the brightest levels they have (relatively) more soft as well as more hard photons. The case of Cyg X-3 (see chapter 9.3.3) illustrates that the assumption of a low-mass donor remains insecure for most of the low-mass X-ray binaries.

Table 9.5. Position, pulse period, characteristic age ($\tau_c \equiv P/(2\dot{P})$, magnetic field strength, orbital period and eccentricity, and companion mass, for representative radio pulsar binaries. The companion masses marked $*$ were calculated for an assumed inclination of 60°.

position	$P_{\rm pulse}$ (ms)	$\log \tau_c$ (yr)	$\log B$ (G)	P (d)	e	M_c ($M_\odot$)
high-mass binary radio pulsars						
1534 + 12	37.9	8.4	10.0	0.42	0.2737	1.36
1913 + 16	59.0	8.0	10.4	0.32	0.6171	1.39
0655 + 64	195.6	9.7	10.1	1.03	<0.00005	>0.7
2303 + 46	1066.4	7.5	11.9	12.34	0.6584	1.5
low-mass binary radio pulsars						
1957 + 20	1.6	9.2	8.2	0.38	<0.001	0.02
1831 − 00	521.0	8.8	10.9	1.81	<0.005	0.07*
J0437 − 47	5.8	8.9	8.9	5.74	0.000018	0.17*
1855 + 09	5.4	9.7	8.5	12.33	0.000021	0.23
1953 + 29	6.1	9.5	8.6	117.35	0.00033	0.22*
0820 + 02	864.9	8.1	11.5	1232.40	0.0119	0.23*
antediluvian[a] radio pulsars						
1259 − 63	47.8			1236.8	0.870	Be
1820 − 11[b]	279.8	6.5	11.8	357.8	0.795	0.8*
single recycled radio pulsars						
1937 + 21	1.6	8.4	8.6			
1257 + 12[c]	6.2					

[a] i.e. in an evolutionary stage preceding mass transfer
[b] this pulsar is tentatively listed as antediluvian; alternatively, this system may be a high-mass binary radio pulsar
[c] this pulsar has three, possibly four planets.

9.3.3 Peculiar X-ray binaries

Pulsars with low-mass donors. Whereas most X-ray pulsars have O or B star companions, some have low- or intermediate-mass companions. The best known of these is Her X-1, which has a $\approx 2\,M_\odot$ companion, which is slightly evolved. Its age is therefore in excess of $\approx 5 \times 10^8$yr, and Her X-1 is an excellent example of an old neutron star with a strong magnetic field. The binary is also striking in being removed from the Galactic Plane, at $|z| \approx 3$ kpc. The X-ray pulsar 4U1626-67 has a companion in a ≈ 40 min orbit, whose mass must be less than $0.1\,M_\odot$. For some other pulsars, including 1E2259+59, there is no sign of any companion. It has been suggested that these are single, accreting from a disk; or that they do not accrete, but have very high magnetic fields.

Radio sources. The X-ray source 3A1909+05, with optical counterpart SS 433, is located in a shell of radio emission. The optical and X-ray spectra of this source show emission lines from a jet with velocity $v \approx 0.26c$, which precesses in about 165 days. The jet is detected directly in Very Long Baseline Interferometry radio observations. It is not clear whether the X-ray source is a neutron star or a black hole. Cyg X-3 has a 4.8 hr orbital period and was classified as a low-mass X-ray binary, until an infrared spectrum was obtained which shows the strong and broad Balmer emission lines characteristic of a Wolf Rayet star. Cyg X-3 has a double radio jet. Cir X-1 is another X-ray source with a radio jet, and is

remarkable for the sudden, extreme surges of the X-ray flux, possibly related to the periastron passage of the donor star.

The first *bursting pulsar* is a very bright transient which shows both pulses and bursts. The bursts are not thermonuclear, but probably due to variation in the accretion onto the neutron star. The second bursting pulsar is also a transient. Its bursts are genuine thermonuclear bursts. Its pulse period is very short, so that we may observe in this system a progenitor of a binary radio pulsar.

9.3.4 Binary radio pulsars

In the last decade, an increasing number of radio pulsars have been discovered in binaries. Two of these pulsars have a companion which is a massive O or B star. Most of the others have a companion believed to be a neutron star or a white dwarf. The pulsars in these other binaries are called recycled radio pulsars, and are generally characterized by short pulse periods, $P \gtrsim 1.5\,\mathrm{ms}$, and very low period derivatives, $P/\dot{P} \gtrsim 10^8\mathrm{yr}$, as compared to the pulse periods and period derivatives of ordinary radio pulsars, which have $P \sim 1\,\mathrm{s}$ and $P/\dot{P} \lesssim 10^7\mathrm{yr}$.

The pulse periods of binary radio pulsars vary with the orbital motion, which provides an indication of the mass of its companion. In three close binaries with two neutron stars, and one binary with a white dwarf and a neutron star, general relativistic effects allow accurate mass determinations. In some binaries, the companion to the recycled pulsar has a mass $M_c \gtrsim 1\,M_\odot$, and – with one exception – these orbits are eccentric. In the other binaries the mass of the companion is lower, $M_c \sim 0.2\,M_\odot$, and the orbits are (almost perfectly) circular (Fig. 9.3). As we will see, the first are thought to have evolved from high-mass X-ray binaries, the latter from low-mass X-ray binaries.

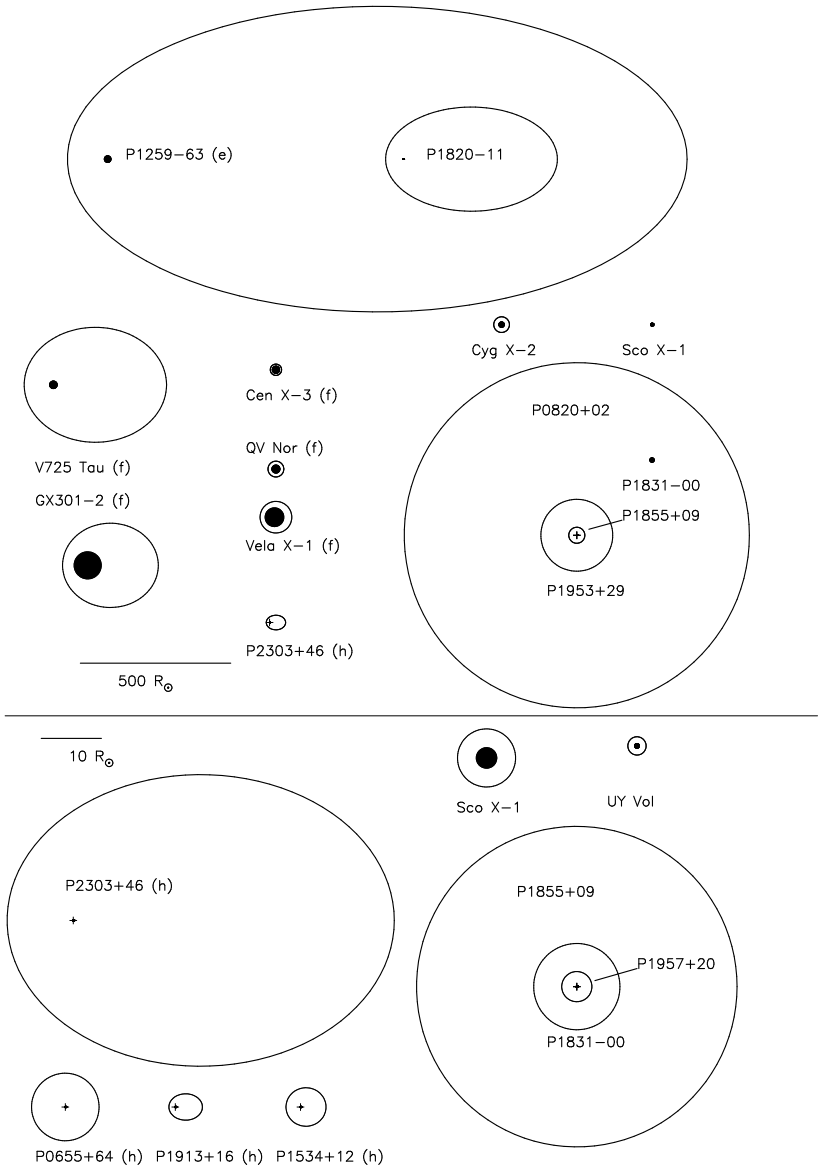

Figure 9.3. Drawing – to scale – of orbits of binaries with compact stars. An example of a massive binary in which one star has already exploded is PSR1259-63. Once the neutron star captures mass from its companion, it becomes an X-ray source like V725 Tau or GX301−2, which after spiral-in may form a binary with a recycled radio pulsar accompanied by a massive white dwarf (PSR0655+64) or after a second supernova by a second neutron star (PSR1913+16). PSR1820−11 may have a low-mass main-sequence companion, and evolve into a low-mass X-ray binary like Cyg X-2, which in turn may form a binary in which a recycled radio pulsar is accompanied by an undermassive white dwarf (PSR1855+09). (e,f,h): see Figure 11.1.

Chapter 10

Violent evolution processes

Two important processes can have a dramatic effect on a binary system, leading to drastic changes in its orbital parameters. In massive binaries, the supernova explosion of one of the stars causes sudden mass loss from the binary and probably also imparts a kick velocity to the remnant. The second process, common-envelope evolution and spiral-in, can affect binaries of all masses. Both these processes introduce major uncertainties in the evolution of binaries containing compact objects.

10.1 Mass loss in a supernova explosion

A neutron star or black hole can be formed from a massive star via a supernova explosion. The envelope of the exploding star is expelled. In a binary the loss of the envelope mass changes the binary parameters. To estimate this effect in a simple way, it is often assumed that the explosion occurs in a circular orbit, is instantaneous, and that the position and velocities of the stars are the same after the explosion as before the explosion. This implies that the distance a_i between the two stars before the explosion is the periastron distance after the explosion

$$a_i = (1 - e)a_f \tag{10.1}$$

and that the periastron velocity of the new orbit is the same as the orbital velocity in the pre-supernova orbit:

$$\frac{G(M_1 + M_2)}{a_i} = \frac{G(M_1 + M_2 - \Delta M)}{a_f}\frac{1 + e}{1 - e} \tag{10.2}$$

Substituting eq. (10.1) in eq. (10.2) gives the eccentricity of the post-supernova orbit:

$$e = \frac{\Delta M}{M_1 + M_2 - \Delta M} \tag{10.3}$$

We see that the binary is disrupted ($e > 1$) when more than half of the total mass is lost in the explosion, i.e. when $\Delta M > (M_1 + M_2)/2$.

Because of the mass loss, the velocity of the center of mass of the binary changes by v_s, given by

$$v_s = \frac{M_2 v_2 - (M_1 - \Delta M)v_1}{M_1 + M_2 - \Delta M} = ev_1 \tag{10.4}$$

where v_i is the orbital velocity of the star with mass M_i before the explosion. Massive binaries have small velocities; thus v_s is a good estimate for the system velocity of the binary after the supernova explosion.

If the orbit after the explosion is sufficiently small, it may be circularized by tidal interaction. From conservation of angular momentum, the radius a_c of the circular orbit can be written in terms of the semi-major axis of the eccentric orbit, or of the radius of the pre-supernova orbit

$$a_c = (1 - e^2)a_f = (1 + e)a_i \tag{10.5}$$

In reality, the correctness of the assumptions made to derive eqs. (10.1–10.5) is rather doubtful. Wide binaries are expected to have initially eccentric orbits. And from measurements of velocities of single radio pulsars, it appears that a single neutron star may receive an appreciable kick velocity at its birth, of several hundred km/s. It may be expected that a neutron star formed in a binary will also obtain a kick velocity at birth. This velocity can have an arbitrary direction and its effect on the orbit is therefore unpredictable. The presence of kick velocities introduces a major uncertainty in the evolution of a binary in which one star undergoes a supernova explosion.

10.1.1 Supernova explosion in an eccentric orbit

In an eccentric orbit, the relative velocity of the two stars when their distance to one another is r is given by

$$v^2 = G(M_1 + M_2)\left(\frac{2}{r} - \frac{1}{a}\right) \tag{10.6}$$

Denote the supernova progenitor mass with M_1, and the pre-explosion semi-major axis with a, and combine eq. (10.6) with a similar equation for the post-explosion orbit, with a compact star of mass $M_{1\rm n}$ and semi-major axis $a_{\rm n}$. Assuming that the instantaneous position r is not changed by the explosion, we then may write the ratio $a/a_{\rm n}$ as

$$\frac{a}{a_{\rm n}} = \frac{2a}{r} - \left(\frac{v_{\rm n}}{v}\right)^2 \frac{M_1 + M_2}{M_{1\rm n} + M_2}\left(\frac{2a}{r} - 1\right) \tag{10.7}$$

where $v_{\rm n}$ is the relative velocity between the two stars immediately after explosion.

The binary will be disrupted if the right hand side of eq. (10.7) is zero, which is the case for

$$\frac{r_{\rm d}}{2a} = 1 - \left(\frac{v}{v_{\rm n}}\right)^2 \frac{M_{1\rm n} + M_2}{M_1 + M_2} \tag{10.8}$$

$r_{\rm d}$ must be on the pre-explosion orbit, i.e. $1-e < r_{\rm d}/a < 1+e$, with e the eccentricity of the pre-explosion orbit. If the value for $r_{\rm d}/a$ found with eq. (10.8) is less than $1 - e$, e.g. when virtually no mass is lost, then the binary remains bound at all pre-explosion radii. If it is larger than $1 + e$, e.g. when virtually all mass is lost, then the binary is disrupted at all radii.

For intermediate values of $r_{\rm d}/a$, the binary will be disrupted at all $r < r_{\rm d}$, and thus the probability that this will happen is given by the fraction of the time that $r < r_{\rm d}$ in the binary orbit. We calculate this fraction by writing r in terms of the eccentric anomaly $\mathcal{E}$ (see Chapter 2)

$$r = a(1 - e\cos\mathcal{E}) \tag{10.9}$$

The eccentric anomaly may be related to the mean anomaly $\mathcal{M}$, which progresses linearly with time, via the equation of Kepler

$$\mathcal{M} = \mathcal{E} - e\sin\mathcal{E} \tag{10.10}$$

To calculate the probability that the supernova will dissolve the binary, we start by calculating $r_{\rm d}/a$ with eq. (10.8), and check whether $1 - e < r_{\rm d}/a < 1 + e$. If so, we continue by calculating the eccentric anomaly $\mathcal{E}_{\rm d}$ corresponding to $r_{\rm d}$ with eq. (10.9), and find the probability that the binary will be disrupted as the probability that the two stars are found at an r between periastron and $r_{\rm d}$ from eq. (10.10) as

$$\Pi_{\rm d} = \frac{\mathcal{E}_{\rm d} - e\sin\mathcal{E}_{\rm d}}{\pi} \tag{10.11}$$

In Fig. 10.1 the probability of survival, $\Pi_{\rm s} \equiv 1 - \Pi_{\rm d}$ is illustrated for a binary with initial semi-major axis of $100\,R_\odot$, in which a $10\,M_\odot$ star explodes to leave a $1.34\,M_\odot$ neutron star, and where the velocity

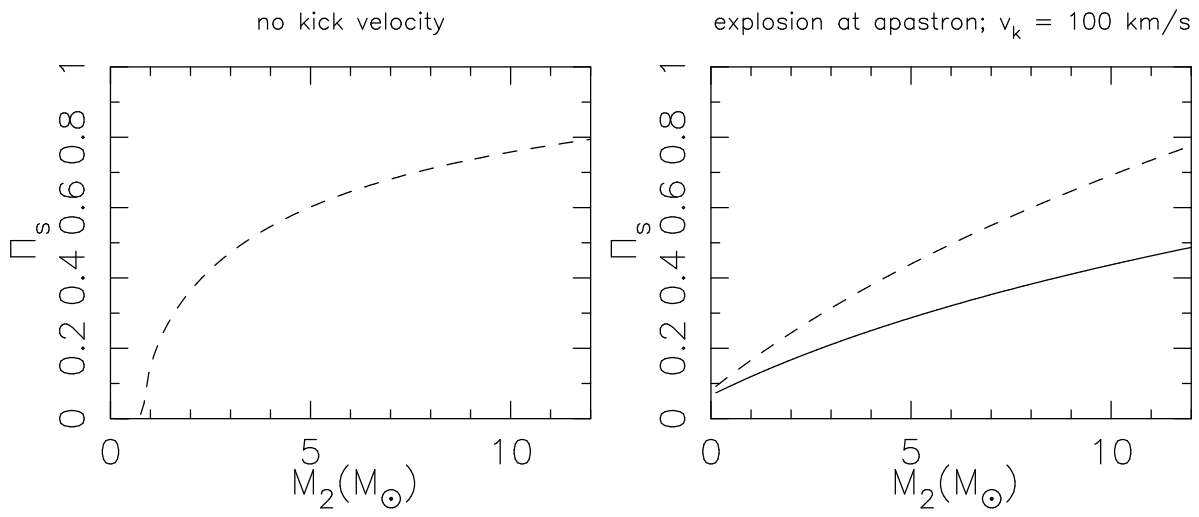

Figure 10.1. The probability Π_s, as a function of the mass M_2 of the non-exploding star, that the binary remains bound after a supernova explosion in which a $10\,M_\odot$ star leaves a $1.34\,M_\odot$ neutron star. (Left) without kick velocity in an eccentric orbit with $e = 0.6$. (Right) for the case in which the neutron star receives a kick velocity of $v_k = 100$ km/s in a circular orbit with $a = 100\,R_\odot$ (solid line) and in an orbit with $e = 0.6$ in which the explosion occurs at apastron (dashed line).

is unchanged: $v_n = v$, as a function of the companion mass M_2. For an initial circular orbit, eq. (10.9) shows that the binary is always disrupted for $M_2 < M_{2\rm crit} = 7.32\,M_\odot$, and always remains bound for $M_2 > M_{2\rm crit}$. For an initial orbit with eccentricity $e = 0.6$, we find that there is a finite probability that the binary survives down to very low companion masses, or that it is disrupted up to relatively high companion masses. The lowest possible companion mass for which the binary can remain bound is found by equating the pre-explosion velocity at apastron to the escape velocity after the explosion, at the same position:

$$v^2 = \frac{G(M_1 + M_2)(1-e)}{a(1+e)} = \frac{2G(M_{1n} + M_2)}{a(1+e)} \quad \Rightarrow \quad M_2 = \frac{(1-e)M_1 - 2M_{1n}}{1+e} \tag{10.12}$$

For the example shown in Fig. 10.1 this minimum mass is $M_2 = 0.825\,M_\odot$. Thus, in the absence of velocity kicks, even very low-mass stars have a finite probability of surviving the supernova explosion of their companion – after all, in an eccentric orbit more time is spent near apastron than near periastron.

10.1.2 Supernova with velocity kick

The calculations that we just discussed would lead to the conclusion that there could be many wide binaries in which a neutron star is accompanied by a low-mass companion, i.e. many radio pulsars would have an optical counterpart. As this appears not to be the case, we must conclude that most neutron stars acquire a kick velocity v_k at birth, which is added to the pre-explosion orbital velocity:

$$v_n^2 = v^2 + v_k^2 + 2vv_k\cos\theta \equiv (1 + f^2 + 2f\cos\theta)v^2 \tag{10.13}$$

where θ is the angle between the kick velocity and the orbital velocity before explosion, and where we have written the kick velocity in units of the pre-explosion velocity, $v_{\rm kick} \equiv fv$. This equation may be entered into eq. (10.8) to check whether the supernova explosion dissolves the binary in the presence of a kick.

To illustrate the effect of a kick we consider an explosion at apastron. The binary remains bound if the post-explosion velocity is less than the escape velocity:

$$(1 + f^2 + 2f\cos\theta)\frac{G(M_1 + M_2)(1-e)}{a(1+e)} \leq \frac{2G(M_{1\mathrm{n}} + M_2)}{a(1+e)} \quad \Rightarrow$$

$$\cos\theta \leq \cos\theta_{\mathrm{crit}} \equiv \frac{1}{2f}\left(\frac{2(M_{1\mathrm{n}} + M_2)}{(M_1 + M_2)(1-e)} - 1 - f^2\right) \tag{10.14}$$

The probability for this to happen is given by the probability that $\theta \geq \theta_{\mathrm{crit}}$, which for arbitrary direction of the kick is given by

$$\Pi_{\mathrm{s}} = \left(\int_{\theta_{\mathrm{crit}}}^{\pi} \sin\theta d\theta\right) / \left(\int_0^{\pi} \sin\theta d\theta\right) = \frac{1 + \cos\theta_{\mathrm{crit}}}{2} \tag{10.15}$$

and may be found directly from eq. (10.14), as illustrated in Fig. 10.1.

10.2 Common-envelope evolution

Two different circumstances can cause the companion of the mass-losing star to find itself engulfed by the envelope of the donor. The first of these is dynamically unstable mass mass transfer, which ensues when the donor cannot shrink fast enough to stay within its Roche lobe (Sect. 7.3). This usually occurs when the donor has a deep convective envelope (late case B and case C) and is of similar mass or more massive than its companion, or when the donor has a radiative envelope (early case B) but is much more massive than its companion, by a factor $\gtrsim 4$. The second circumstance arises when the spin angular momentum is more than $\frac{1}{3}$ times the orbital angular momentum, which causes tidal interaction to become unstable and the companion is literally dragged into the donor's envelope by tidal forces. This can occur when the mass ratio is very large.

Once the companion is inside the donor's envelope, the friction between the motion of the companion and the envelope removes angular momentum from the orbital motion, and releases energy. Thus, the orbit shrinks, and the envelope is brought into rotation and heated. This process continues until enough energy is added to the envelope to expel it. Alternatively, the companion star may spiral-in until it merges with the core of the mass donor.

This process, known as common-envelope evolution, was originally proposed in 1976 by B. Paczyński as an explanation for the existence of compact objects in very short-period binaries, such as cataclysmic variables, low-mass X-ray binaries and double white dwarfs (Chapter 9). The formation of such compact binaries requires the initial orbit to be wide enough for the progenitor of the compact object to expand to red giant dimensions and thus requires a substantial loss of orbital energy and angular momentum.

The outcome of a common envelope is often estimated based on the picture of conversion of orbital energy into binding energy of the envelope, which may or may not be thrown off eventually depending on how much orbital energy is available. We can measure the efficiency of the CE process as

$$\alpha_{\mathrm{CE}} = \frac{\Delta E_{\mathrm{bind}}}{\Delta E_{\mathrm{orb}}} \tag{10.16}$$

where

$$\Delta E_{\mathrm{orb}} = \frac{GM_{\mathrm{a}}M_{\mathrm{c,d}}}{2a_{\mathrm{f}}} - \frac{GM_{\mathrm{a}}M_{\mathrm{d}}}{2a_{\mathrm{i}}} \tag{10.17}$$

and $\Delta E_{\rm bind}$ is estimated as the binding energy of the envelope at the start of the CE process, i.e. as the binding energy of the donor envelope when it first fills its Roche lobe[1]:

$$\Delta E_{\rm bind} = \int_{M_{\rm c,d}}^{M_{\rm d}} \left(\frac{Gm}{r} - U \right) dm \tag{10.18}$$

$$\equiv \frac{GM_{\rm d}M_{\rm env,d}}{\lambda R_{\rm L,d}}. \tag{10.19}$$

The dimensionless parameter λ is a measure of the relative density distribution within the envelope, and of the contribution of internal energy (U) to the binding energy. We can then formally compute the ratio of final to initial separation as

$$\frac{a_{\rm f}}{a_{\rm i}} = \frac{M_{\rm c,d}}{M_{\rm d}} \frac{M_{\rm a}}{M_{\rm a} + 2M_{\rm env,d}/(\alpha_{\rm CE}\lambda r_{\rm L,d})} \tag{10.20}$$

where $r_{\rm L,d} = R_{\rm L,d}/a_{\rm i}$ is the relative Roche-lobe size of the the donor at the start of the CE, a function only of $M_{\rm d}/M_{\rm a}$. Usually the second term in the denominator of eq. (10.20) dominates over the first term, in which case we can simplify the equation to

$$\frac{a_{\rm f}}{a_{\rm i}} \approx \tfrac{1}{2}\alpha_{\rm CE}\lambda\, r_{\rm L,d}\, \frac{M_{\rm c,d}M_{\rm a}}{M_{\rm d}M_{\rm env,d}}. \tag{10.21}$$

The outcome of the common envelope phase is seen to depend on the product $\alpha_{\rm CE}\lambda$. The parameter λ can be calculated from a stellar structure model of the star at the moment it fills its Roche lobe. This can be done with reasonable accuracy, the main uncertainty being the exact boundary between the core and the envelope that will be ejected.

Two approaches have been taken to determine the efficiency parameter $\alpha_{\rm CE}$ of the common envelope process. Theoretically, $\alpha_{\rm CE}$ can be calculated from a three-dimensional hydrodynamic calculation of the spiral-in process. Much effort has one into such calculations, which are very challenging owing to the enormous range of spatial and temporal scales involved in the late phase of a common envelope. Realistic calculations must also include the effects of turbulence and radiative transfer, which is not yet feasible. The limited 3D hydrodynamical calculations done so far (which do not include the entire process from start to end) indicate values of $\alpha_{\rm CE} < 1$. These results should not be taken too literally yet. In particular the calculations do not take into account that, once the envelope has been spun up and the spiral-in has slowed down sufficiently, additional energy sources may aid in ejecting the envelope, such as nuclear power, accretion power or dynamical energy in envelope pulsations.

Another approach is to determine $\alpha_{\rm CE}$ observationally. Central binaries of planetary nebulae are very good objects for such a study, because the 'smoking gun' of the nebula shows that such binaries have only just emerged from a common envelope, i.e. they represent the conditions immediately following the spiral-in. The determination goes as follows. If the white dwarf is of low mass, $\lesssim 0.45\,M_\odot$, it must have formed as the helium core of a low-mass star on the red giant branch, which obeys a core-mass radius relation (Sect. 6.2.3). The mass of the white dwarf thus more or less fixes the size of the Roche lobe at the onset of the common envelope, such that the ratio $a_{\rm f}/a_{\rm i}$ can be determined from observed quantities. Applying eq. (10.20) to systems with a low-mass white dwarf and a main-sequence or other white-dwarf companion shows that $\alpha_{\rm CE}$ is in the range 0.2 to 1.

However, it has become clear that not all binaries for which dynamically unstable mass transfer is expected undergo spiral-in. Several symbiotic binaries and barium-star binaries have periods of a few hundred days, too short to have avoided unstable Roche-lobe overflow but too long to have experienced strong spiral-in. Furthermore, if one applies the technique described above in combination with eq. (10.20) to the first white dwarf formed in a double white-dwarf binary, one often finds *negative* values

[1]Note that others, e.g. Iben & Livio (1993), assume that the envelope has already expanded to a radius of $2a_{\rm i}$ when the CE phase starts.

of $\alpha_{\rm CE}$! The masses of the white dwarfs in such systems are often very similar, which means (applying the core-mass radius relation) that the separation did not change drastically between the formation of the first and the second white dwarf (Nelemans et al., 2000). This is inconsistent with either conservative mass transfer (which expands the orbit) or spiral-in. It appears that some binaries for which a common envelope is expected are capable of evolving very non-conservatively, but without strong orbital energy and angular momentum losses. How this process works is not understood. Additional energy sources are needed, such as nuclear energy, but this requires much longer timescales than the $\lesssim 10^3$ years normally associated with a common enevelope.

Exercises

10.1 The system V635 Cas (see Table 9.4) is an example of a Be X-ray binary. Assume a canonical mass of 1.35 $M_\odot$ for the neutron star and a mass of 15 $M_\odot$ for the Be star (typical of the Be components in such binaries).

(a) Why is it reasonable to assume a circular pre-supernova orbit in this system?

(b) Assuming the supernova was symmetric, compute the mass of the neutron-star progenitor just before the explosion.

10.2 Consider the example binary system discussed and plotted in Fig. 10.1. Assuming the pre-explosion orbit is circular with $a = 100\,R_\odot$, compute the maximum kick velocity for which a star of 1 $M_\odot$ can survive the supernova explosion of its 10 $M_\odot$ companion without the binary being disrupted.

10.3 Her X-1 is an X-ray binary with an orbital period of 1.7 days in which a main-sequence or subgiant star of 2.0 $M_\odot$ is transferring mass to its neutron star companion, which is observed as an X-ray pulsar. Fig. 10.2 shows two possible evolution scenarios.

The first one (the standard scenario) starts with a massive NS progenitor (10 $M_\odot$) and a 2 $M_\odot$ companion in a wide orbit (stage 1), which evolves via case C mass transfer (stage 2) and spiral-in into a close binary consisting of the helium core of the progenitor and the unchanged 2 $M_\odot$ companion with a short orbital period (stage 3). The helium core explodes and leaves a 1.4 $M_\odot$neutron star in an eccentric orbit (stage 4). Finally, after tidal interaction has circularized the orbit, Roche-lobe overflow starts and an X-ray binary with the observed parameters is formed (stage 5).

(a) Reconstruct this evolution scenario by filling in the missing values in the Figure, using the formulae encountered in the lectures. Also compute the eccentricity induced by the supernova at stage 4. Assume the SN explosion was symmetric (i.e. ignore the possible kick velocity) and assume that the spiral-in can be described by the energy balance prescription with $\alpha_{\rm CE} = \lambda = 1$. Also compute the system velocity of the binary after the explosion.

(b) The second scenario (accretion-induced collapse) involves an intermediate-mass progenitor, which initially forms a massive white dwarf (1.35 $M_\odot$) after case C mass transfer and spiral-in. When the companion fills its Roche lobe, it transfers mass to the white dwarf and pushes it over the Chandrasekhar limit when its mass is 1.44 $M_\odot$ (stage 4). A neutron star of 1.26$M_\odot$ is formed (stage 5). Compute the eccentricity and system velocity for this case, assuming no kick occurs.

Note: Her X-1 is at a distance of $z \approx 3$ kpc from the Galactic plane. If it was born in the plane, where the high-mass progenitors of neutron stars are, then the velocity as calculated in (b) is too low to carry it to its current position. Therefore accretion-induced collapse is not an option for Her X-1. To show this conclusively one must also investigate scenarios with kick velocities.

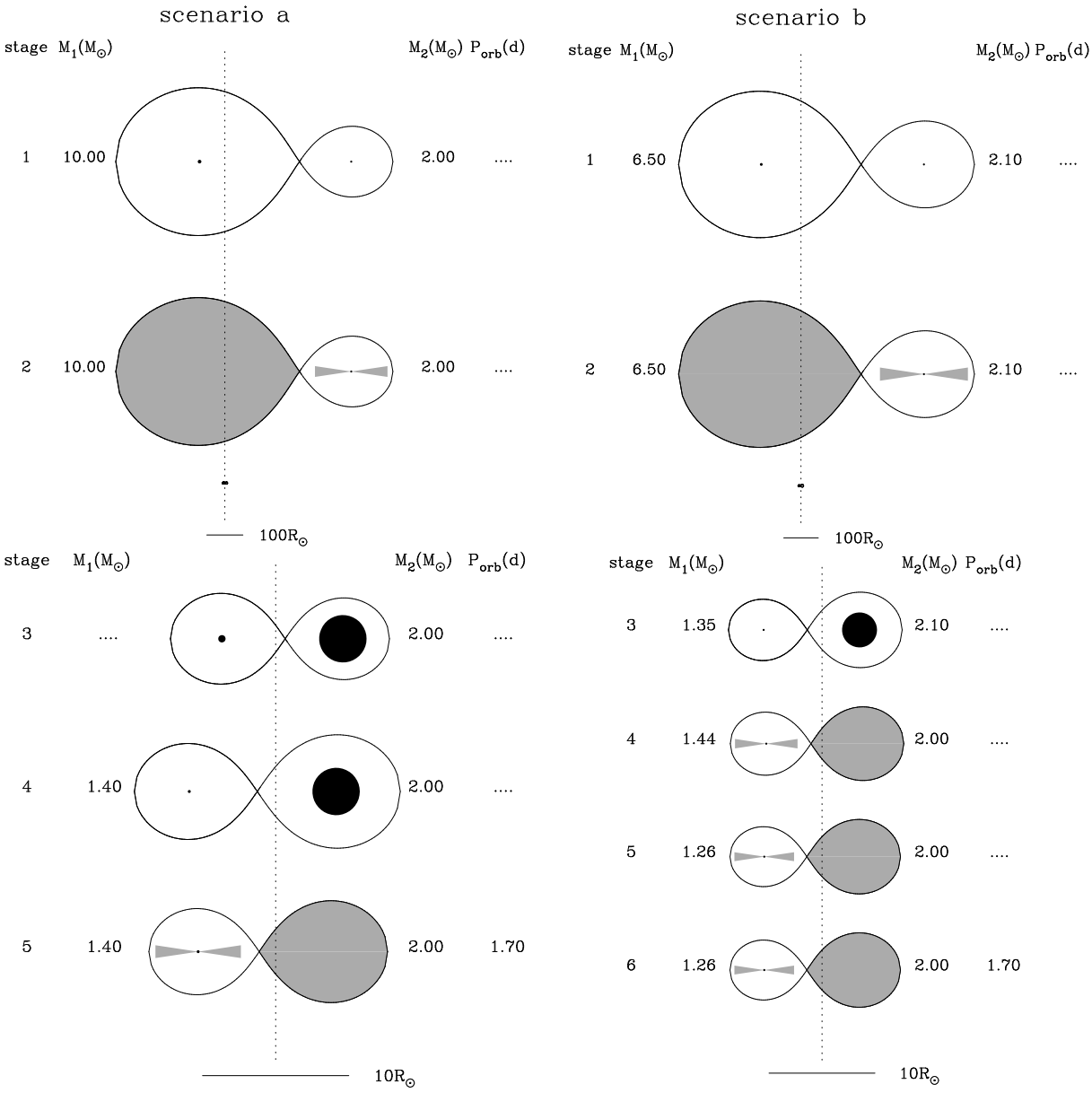

Figure 10.2. Drawing (to scale) of two scenarios for the evolution of Her X-1. Left: the standard scenario involving a massive primary; right: the accretion-induced collapse scenario. Note the change in scale after the spiral-in phase (stage 3).

Chapter 11

Origin and evolution of X-ray binaries

11.1 Formation and evolution of high-mass X-ray binaries

The observed presence of a neutron star in a binary poses the following problem. According to the theory of stellar evolution, it is always the more massive star in a binary that explodes first as a supernova. According to eq. (10.3) this means that the binary is disrupted ($e > 1$) by the supernova explosion, unless the masses of the two stars are very close to one another (more specifically: $M_1 > M_2 > M_1 - 2M_{\rm NS}$, where $M_{\rm NS}$ is the mass of the compact remnant, i.e. the neutron star). One therefore does not expect to find (many) binaries with a neutron star. Two possible solutions have already been discussed in Sect. 10.1: the supernova can occur at apastron of an eccentric orbit (eq. 10.12) and the new neutron star may be born with a kick velocity (eq. 10.14). Most important, however, is the possibility that the more massive star becomes the less massive star before it explodes as a result of mass transfer. We discuss three scenarios for this.

11.1.1 Origin of the Be X-ray binaries: pre-supernova case B mass transfer

The evolution of a massive binary into a Be/X-ray binary is illustrated in Figure 11.1. In this example a binary starts out with 12 and 8 $M_\odot$, and an orbital period $P_{\rm orb} = 50$ days. The 12 $M_\odot$ star evolves first and expands after it exhausts its hydrogen, filling its Roche lobe when it crosses the Hertzsprung gap (Fig 11.1b). The binary thus evolves according to Case B, see Sect. 8.2. Since the more massive star still has a radiative envelope at this point, and the mass ratio is not far from unity, mass transfer may be conservative as has been assumed in this example. The orbital period decreases until the masses are equal (Fig 11.1c) after which the orbit expands. Mass transfer occurs on the thermal timescale of the donor star until almost the entire envelope has been transferred to the companion star; only then does the equilibrium radius of the donor star become smaller than its Roche lobe (Sect. 8.2). The 8 $M_\odot$ star has gained appreciably in mass, and rotates rapidly, due to the accretion of angular momentum with the mass. The result of the first phase of mass transfer is a binary in which the almost naked helium core of the initially more massive star is in a wide orbit around an Oe or Be star companion.

The core continues its evolution, and after a short time explodes as a supernova, leaving a neutron star of 1.35 $M_\odot$ (Fig. 11.1e). The sudden mass loss leads to an eccentricity of $e = 0.08$ and a velocity of the center of mass of the new binary of $v_s = 5.9$ km/s for an assumed symmetric explosion, according to eqs. (10.3–10.4). The neutron star may catch matter from the dense equatorial wind of the Be star and appear as an X-ray source. The wind of the Be star, too, often is transient; thus the binary is often a transient source of hard X-rays. The Be stars in Be X-ray binaries have inferred masses between 8 and 20 $M_\odot$. The upper limit is thought to be due to a selection effect: more massive stars have such strong winds that their rotation slows down quickly, and they cease having the strong equatorial outflows characteristic of Be stars. Accretion from the fast and tenuous winds of O stars is much less efficient,

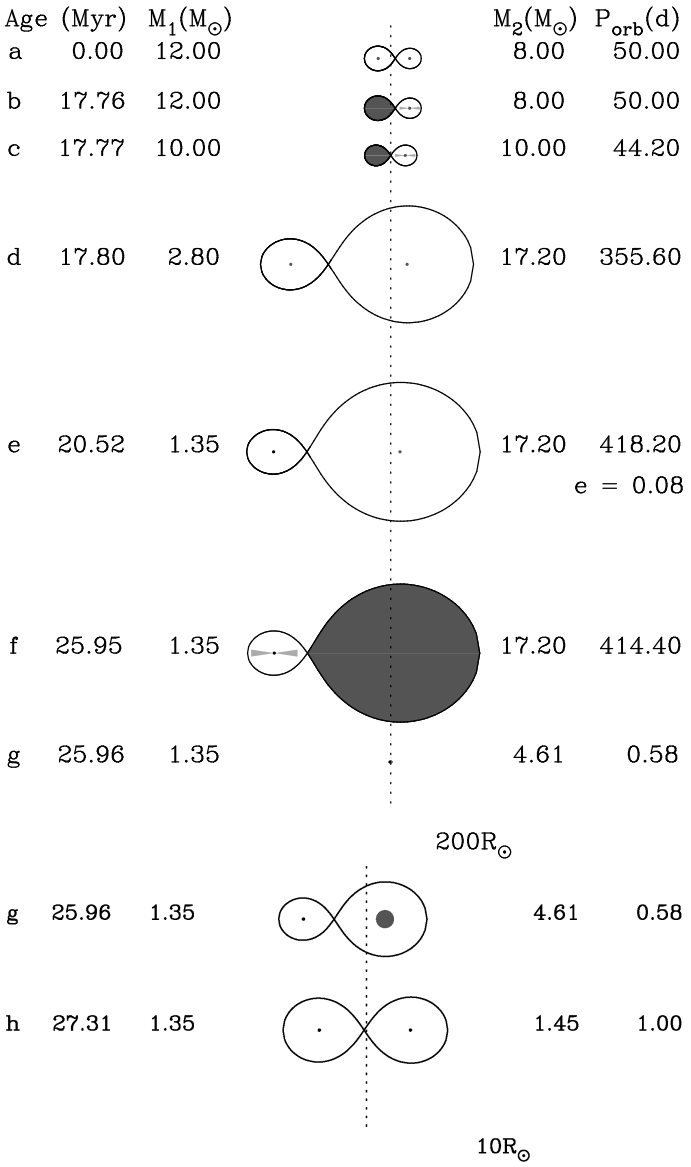

Figure 11.1. Conservative evolution of high-mass binary into a Be X-ray binary, and then into a binary radio pulsar. For explanation see text. Note the change of scale at phase g.

and does not produce a strong X-ray source unless the orbital period is $\lesssim 10$ days.

In early computations of binary evolution it has mostly been assumed that the helium core unwrapped by mass transfer evolves pretty much in the same way as it would have done inside the whole star. By computing the evolution of unwrapped cores explicitly several authors have shown that this assumption is not correct. In particular, even the cores of very massive stars, which would have evolved into a black hole inside the full star, can evolve into a neutron star instead when the star loses its envelope at an early evolutionary stage, due to the strong Wolf-Rayet mass loss of such exposed cores. This explains why no Be X-ray binary (formed via case B mass transfer) contains a black hole. An important consequence is that one can no longer transfer conclusions about the progenitor mass of a black hole from single-star evolution to binary evolution or vice versa.

Evolution into high-mass binary pulsars Overflow via the inner Lagrangian point starts when the companion reaches its Roche lobe (Fig 11.1f). The extreme mass ratio almost certainly causes the mass transfer to be dynamically unstable as the orbit shrinks rapidly (see eq. 7.9), and the neutron star eventually will plunge into the envelope of its companion. In the case shown in Figure 11.1, the spiral-in leads

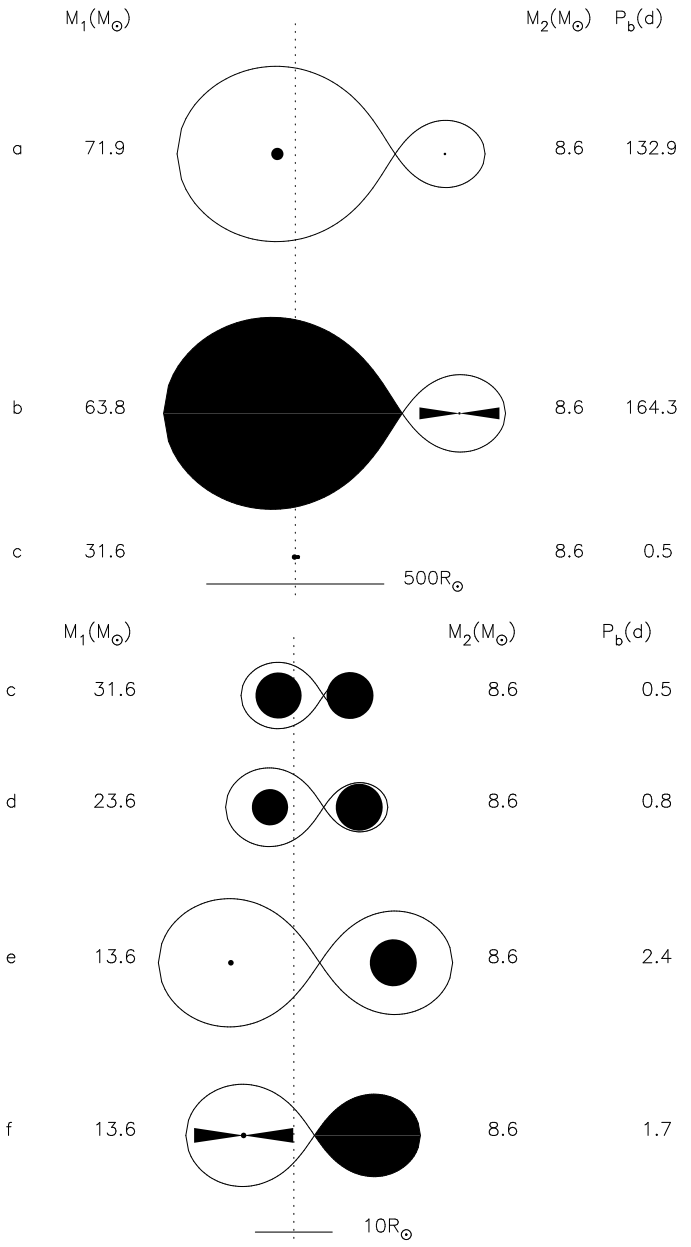

Figure 11.2. Drawing – to scale – of the evolution of a high-mass binary with a close initial orbit. For explanation see text; note the change in scale at phase c. The 8.6 $M_\odot$ star in phase c only barely fits in its Roche lobe. The final binary is modelled on LMC X-3.

to a very close binary consisting of the neutron star and the core of the Be star (Fig. 11.1g). If the helium core has too low a mass to evolve into a supernova, it will cool into a white dwarf, and the resulting binary looks like the one in which PSR 0655 + 64 is accompanied by a relatively massive white dwarf. In that case, the orbit retains the circular shape it obtained during spiral-in. Alternatively (as shown in Fig. 11.1h), continued evolution of the core leads to a second supernova explosion, which may lead to the formation of a high-mass radio pulsar binary like PSR 1913 + 16, consisting of two neutron stars in an eccentric orbit; or which may disrupt the binary. In the example shown, a symmetric explosion would disrupt the binary and a suitably aimed kick velocity is needed to produce a binary pulsar.

11.1.2 Origin of the supergiant X-ray binaries: case A mass transfer or spiral-in

Two very different scenarios have been discussed to explain the existence of the ‘standard’ high-mass X-ray binaries with a supergiant companion in a close orbit. The first scenario is similar to the one

sketched above for the Be/X-ray binaries, involving (quasi)conservative mass transfer. Three effects conspire to keep the orbital period much shorter than in a Be/X-ray binary. First, the ratio of core mass to envelope mass increases with stellar mass (according to eq. 8.1) so that in a more massive binary relatively less mass is transferred, which results in less orbital expansion after conservative mass transfer (see Exercise 8.3). Second, many supergiant X-ray binaries are thought to originate from case A instead of case B, with initially very close orbits. This also explains that a neutron star can be accompanied by a very massive donor, as in the case of the binary Wray 977, in which a $48\,M_\odot$ star transfers mass to a neutron star: such a binary can form by conservative case A mass transfer even if the progenitor of the neutron star had an initial mass as low as $25\,M_\odot$. Third, and in contrast, substantial loss of mass and angular momentum during case A mass transfer is needed to explain the properties of some neutron-star supergiant binaries with $P_{\rm orb} < 10$ days.

The alternative scenario involves a massive and initially very wide binary that undergoes dynamically unstable case C mass transfer. This brings the mass-receiving star inside the envelope of the donor star and initiates a common envelope event (Sect. 10.2). Friction then transfers angular momentum and energy from the orbital motion to the envelope of the mass donor. As a result, the orbit shrinks dramatically, until the envelope is heated so much that it escapes, leaving the core of the donor in orbit around the mass-receiver, or until both stars merge completely. This spiral-in process happens so rapidly, that the mass receiving star accretes only a tiny fraction of the envelope of the donor.

This scenario is discussed especially to explain the formation of black-hole high-mass X-ray binaries such as LMC X-3, as illustrated in Fig. 11.2. The more massive star of the binary loses some mass in a stellar wind before it fills its Roche lobe. The mass transfer is unstable, and a spiral-in ensues, bringing the core of the donor in close orbit around the virtually unchanged receiver (see eq. 10.20; phases b-c in Fig. 11.2). The donor only fits inside its Roche lobe because stars in the LMC, due to their lower metallicity, are smaller at the same mass than stars in our Galaxy. The core loses some more mass in stellar wind as it evolves to a supernova, and forms a black hole (Fig. 11.2c-e).

11.2 Formation of low-mass X-ray binaries

The problem in producing a high-mass X-ray binary, i.e. avoiding a disruption of the binary during the supernova event, holds even more for the low-mass X-ray binaries. Mass loss via a wind of a massive star will not bring its mass below the $1M_\odot$ of a low-mass companion. In order to keep the binary intact, one may have to invoke both a spiral-in phase and a rightly aimed kick velocity of the newly born compact star. An alternative that has been in vogue during the past few years is a quiet supernova explosion, when a white dwarf is pushed over the Chandrasekhar limit and implodes. Yet another alternative is evolution of a multiple system of three or more stars.

11.2.1 Origin of low-mass X-ray binaries via spiral-in

The spiral-in scenario was suggested first by van den Heuvel in 1983. Eqs. (10.20,10.21) show that the initial binary must have been rather wide if a merger is to be avoided. This allows both late case B (i.e. mass transfer starting when the donor is already a red giant with a convective envelope) or case C. To avoid a merger, case C mass transfer is preferred above case B, as the core mass will be higher and the envelope mass smaller. Consider for example a star just massive enough to evolve into a neutron star, with an initial mass of $11\,M_\odot$ which evolves a helium core of $2.5\,M_\odot$ on the giant branch (Fig. 11.3). A $1M_\odot$ companion to this core fits within its Roche lobe provided the semimajor axis is larger than $3.3\,R_\odot$ (Fig. 11.3c). With eq. (10.20) and assuming $\alpha_{\rm CE}\lambda = 1$, we find that this requires a semimajor axis before spiral-in that is $430\,R_\odot$. An $11\,M_\odot$ star indeed expands to fill its Roche lobe in this binary during the first giant ascent before helium ignition, i.e. mass transfer is case B. The main-sequence star is hardly affected by the spiral-in process, and emerges pretty much as it entered.

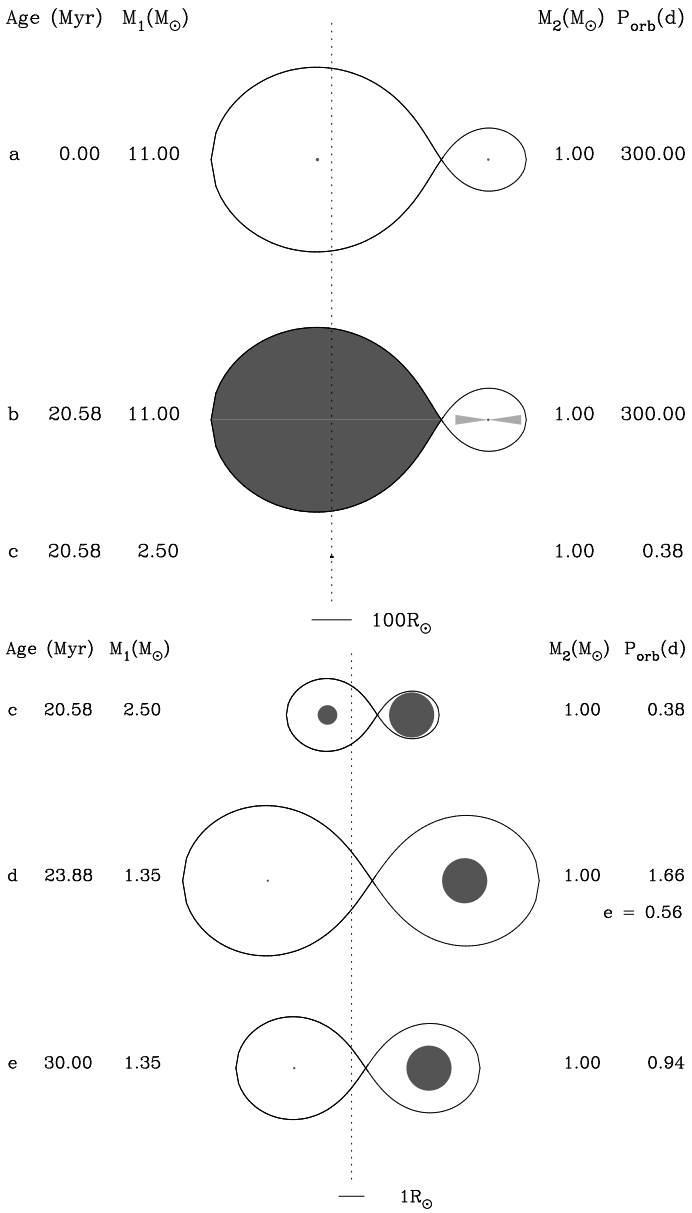

Figure 11.3. Evolution of a massive binary with an extreme mass ratio into a low-mass X-ray binary via a common envelope phase resulting in spiral-in, followed by the supernova explosion of the helium core of the massive star. For explanation see text. Note the change of scale at stage c.

The supernova explosion of the $2.5\,M_\odot$ helium core causes an eccentricity $e = 0.56$, if a $1.35 M_\odot$ neutron star is formed without a kick velocity (Fig. 11.3d). Tides quickly circularize the binary so that it ends up with the low-mass star underfilling its Roche lobe by about a factor 2 (Fig. 11.3e). Angular momentum losses may then bring the $1 M_\odot$ star in contact with its Roche lobe, provided the post-supernova orbit is not too wide (see Sect. 11.3). In a system with a longer orbital period, mass transfer can start only after the $1 M_\odot$ star evolves away from the main sequence, and expands into a (sub)giant. The boundary between these two cases depends on the mechanism for loss of angular momentum.

Thus, the spiral-in scenario does allow the formation of low-mass X-ray binaries. However in reality the scenario is more complicated than sketched above. The crucial moment in the evolution is the moment of the supernova explosion. If the binary is to remain bound, not too much mass must be lost from the system with the explosion (see eq. 10.3). This may be the case if the core of the neutron star progenitor is not too massive, i.e. if the progenitor itself is not too massive, as in the example just described. However, such relatively low-mass helium stars expand and fill their Roche lobes again after exhausting helium in their centre, leading to a renewed phase of (unstable) mass transfer to the compan-

ion. Therefore either the initial orbit must be even wider, allowing two consecutive spiral-in phases, or the neutron-star progenitor must be more massive. In that case, a well-directed kick may help to keep the binary bound. Interestingly, collapse of a massive evolved core into a black hole may also make it easier for the binary to remain bound, as a smaller fraction of the mass is expelled in that case.

PSR 1820 – 11 has already been mentioned as a possible high-mass radio pulsar binary. The available observations also allow the companion to the pulsar to be a low-mass main-sequence star; if so, the binary would be a progenitor of a low-mass X-ray binary, along the scenario just sketched.

11.2.2 Origin via accretion-induced collapse

Accretion-induced collapse of a massive white dwarf as a mechanism for the formation of a neutron star was first suggested by Whelan & Iben in 1973. The progenitor of a massive white dwarf must have a mass close to those of direct progenitors of neutron stars. The close binary is therefore formed through a spiral-in, very similar to the spiral-in just described: however, the core that emerges from the spiral in now evolves into a massive white dwarf, and avoids the supernova explosion. When mass transfer is initiated, either by loss of angular momentum or by expansion of the secondary into a (sub)giant, the white dwarf accretes mass until it transgresses the Chandrasekhar limit, at which point it implodes. Little mass is lost in the implosion; most of the loss in fact may come from the change in binding energy, which is roughly:

$$\Delta M \approx \frac{3GM_{\rm WD}{}^2}{5R_{\rm NS}c^2} \approx 0.2M_\odot \tag{11.1}$$

where $M_{\rm WD}$ is the mass of the white dwarf and $R_{\rm NS}$ the radius of the neutron star. The smaller mass loss makes it easier for the binary to survive the supernova explosion. It is often implicitly assumed that the kick velocity is also less for a neutron star formed by white dwarf collapse. As long as the mechanism causing the kick velocity is not known, however, there is no good reason for such an assumption.

Accretion-induced collapse as a mechanism to form a neutron star gained widespread recognition once it was realized that the magnetic field of the radio pulsar in old binaries was still in excess of 10^8G. Combined with the view that the magnetic field of a neutron star decays on a time scale of a few million years, this meant that there must be young neutron stars in old binaries: accretion-induced collapse can achieve this. It has recently become less clear, however, that the magnetic field of neutron stars does indeed decay so rapidly. In the absence of rapid decay of the magnetic field of neutron stars, there is no reason anymore to invoke accretion-induced collapse for the formation of low-mass X-ray binaries.

11.3 Evolution of low-mass X-ray binaries

By combining Kepler's law eq. (2.42) with an expression for the Roche-lobe radius, eq. (6.2), we get an approximate relation between the orbital period and the mass and radius of the Roche-lobe-filling star (see Exercise 6.2):

$$P_{\rm orb} \approx 0.35\,{\rm d}\left(\frac{R_{\rm d}}{R_\odot}\right)^{3/2}\left(\frac{M_{\rm d}}{M_\odot}\right)^{-1/2}\left(\frac{2}{1+q}\right)^{0.2} \approx 9.6\,{\rm hr}\left(\frac{R_{\rm d}}{R_\odot}\right)^{3/2}\left(\frac{M_{\rm d}}{M_\odot}\right)^{-1/2}(1+q)^{-0.2} \tag{11.2}$$

For low-mass donors, when $q \lesssim 0.7$, we can ignore the weak dependence on the mass ratio. Thus, by assuming a mass-radius relation for the donor star, we may determine its mass from the observed orbital period, as summarized in Table 11.1. In Fig 9.1 the known orbital periods for low-mass X-ray binaries are shown.

In stable mass transfer, the radius of the donor equals the radius of the Roche lobe at all times in this process, so that $R_{\rm L} = R_{\rm d}$ and $\dot{R}_{\rm L} = \dot{R}_{\rm d}$. The change in radius of the donor star may be due to internal

Table 11.1. Mass-radius relations and derived mass-orbital-period relations for low-mass X-ray binaries. Valid for donors in thermal equilibrium.

low-mass MS	$R_\mathrm{d}/R_\odot \approx M_\mathrm{d}/M_\odot$	$\zeta_\mathrm{eq} \approx 1$	$P_\mathrm{orb} \approx 9.6\,\mathrm{hr}\,M_\mathrm{d}/M_\odot$
low-mass He-MS	$R_\mathrm{d}/R_\odot \approx 0.2\,M_\mathrm{d}/M_\odot$	$\zeta_\mathrm{eq} \approx 1$	$P_\mathrm{orb} \approx 0.86\,\mathrm{hr}\,M_\mathrm{d}/M_\odot$
white dwarf	$R_\mathrm{d}/R_\odot \approx 0.0115\ (M_\mathrm{d}/M_\odot)^{-1/3}$	$\zeta_\mathrm{eq} = -\frac{1}{3}$	$P_\mathrm{orb} \approx 43\,\mathrm{sec}\,(M_\mathrm{d}/M_\odot)^{-1}$
low-mass red giant	$R_\mathrm{d}/R_\odot \approx 3500\ (M_\mathrm{c,d}/M_\odot)^4$	$\zeta_\mathrm{eq} \approx 0$	$P_\mathrm{orb} \approx 20\,\mathrm{d}\left(\frac{M_\mathrm{c,d}}{0.25M_\odot}\right)^6\left(\frac{M_\mathrm{d}}{M_\odot}\right)^{-1/2}$

evolution of the star, or to the mass-transfer process. Similarly, the change in the Roche radius may be due to the mass-transfer process or to the (spontaneous) loss of orbital angular momentum:

$$\frac{\dot{R}_\mathrm{d}}{R_\mathrm{d}} = \left(\frac{\dot{R}_\mathrm{d}}{R_\mathrm{d}}\right)_\mathrm{ev} + \zeta_\mathrm{eq}\frac{\dot{M}_\mathrm{d}}{M_\mathrm{d}} \qquad \text{and} \qquad \frac{\dot{R}_\mathrm{L}}{R_\mathrm{L}} = \left(\frac{\dot{R}_\mathrm{L}}{R_\mathrm{L}}\right)_\mathrm{aml} + \zeta_\mathrm{L}\frac{\dot{M}_\mathrm{d}}{M_\mathrm{d}} \tag{11.3}$$

where we have used the mass-radius exponents defined in Sect. 7.3. The term $(\dot{R}_\mathrm{L}/R_\mathrm{L})_\mathrm{aml} = \dot{a}/a = 2\dot{J}/J$ according to eq. (7.8) in the absence of mass transfer. Thus we can derive the mass transfer rate $-\dot{M}_\mathrm{d}$ as (remembering that $\dot{M}_\mathrm{d}$ is negative)

$$-\frac{\dot{M}_\mathrm{d}}{M_\mathrm{d}} = \frac{1}{\zeta_\mathrm{eq} - \zeta_\mathrm{L}}\left[\left(\frac{\dot{R}_\mathrm{d}}{R_\mathrm{d}}\right)_\mathrm{ev} - 2\frac{\dot{J}}{J}\right] \tag{11.4}$$

This equation shows that mass transfer may be driven by loss of angular momentum from the binary ($\dot{J} < 0$), or by expansion of the donor star ($\dot{R}_\mathrm{d} > 0$) due to, for example, the ascent of the donor on the (sub)giant branch, or due to irradiation of the donor. We discuss these possibilities in turn.

11.3.1 Evolution via loss of angular momentum

The low-mass X-ray binaries with orbital periods between 80 min and 10 h may have main-sequence donors with masses between $0.1M_\odot$ and $1.0M_\odot$, according to Table 11.1. The evolutionary time scales of such low-mass stars are very long (see eq. 6.5). Since these masses are less than the $1.4M_\odot$ characteristic for a neutron star, the orbit of such a low-mass X-ray binary expands when mass is transferred conservatively from the donor (see eq. 7.9). Unless the donor star expands more than its Roche lobe, this expansion will put an end to the mass transfer. It appears then that angular momentum must be lost from the binary to keep mass transfer going. Two processes have been proposed to provide such orbital angular momentum loss.

Gravitational radiation It was realized by Kraft et al. in 1962 that gravitational radiation provides a sufficiently high loss of angular momentum to drive observable mass transfer in a close binary. According to general relativity the changing quadrupole moment of the orbiting bodies produces gravitational waves that carry energy and angular momentum from the orbit. The loss of angular momentum via gravitational radiation may be written, for a circular orbit:

$$-\left(\frac{\dot{J}}{J}\right)_\mathrm{GR} = \frac{32G^3}{5c^5}\frac{M_1M_2(M_1+M_2)}{a^4} \tag{11.5}$$

(For an eccentric orbit, this should must be multiplied by a function of eccentricity.) The strong dependence on the size of the orbit (a^{-4}) means that this process is only effective in very close binaries: the timescale for angular momentum loss $\tau_\mathrm{GR} = -J/\dot{J}$ becomes comparable or shorter than the Hubble time if $a \lesssim 1\,R_\odot$.

Magnetic braking Single stars of spectral type F or later show signs of magnetic activity (such as starspots and X-ray emission) and their rotation is observed to slow down with age. This is interpreted as loss of angular momentum via their stellar winds. Even though the amount of mass lost in the wind is very small, the concurrent loss of angular momentum may be appreciable because the magnetic field of the star forces the wind matter to corotate to a large distance from the stellar surface. If the donor star in a close binary loses angular momentum in this way, it will not be able to rotate slower, as it is kept in corotation with the orbit by tidal forces. Thus loss of angular momentum is transferred from the donor rotation to the orbital revolution, i.e. the binary loses angular momentum.

The rate of angular momentum loss has been derived approximately as follows. Skumanich found in 1972 that the rotation velocities of single G stars decreases with age as $v_{\rm rot} \approx 5.0\,(t/{\rm Gyr})^{-0.5}\,{\rm km/s}$. Since $\dot{J} = I\dot{\Omega}$ and $v_{\rm rot} = \Omega R$, where Ω is the angular spin frequency of the star, and writing the moment of inertia as $I = k^2 M R^2$, the angular momentum loss should be

$$\dot{J} \approx -4 \times 10^{-29}\,{\rm s/cm^2} \times k^2 M R^4 \Omega^3 \tag{11.6}$$

in cgs units, with $k^2 \approx 0.1$ for a low-mass main-sequence star. In a tidally locked binary, Ω equals the the orbital angular frequency $2\pi/P$. Using Kepler's law we can then write the orbital angular momentum loss due to magnetic braking as

$$-\left(\frac{\dot{J}}{J}\right)_{\rm MB} \approx 4 \times 10^{-30}\,{\rm s/cm^2} \times \frac{G(M_1 + M_2)^2 R_1^4}{M_2\, a^5} \tag{11.7}$$

According to this formula angular momentum loss due to magnetic braking increases strongly with decreasing separation, due to its strong dependence on stellar rotation rate. However, this result relies on extrapolating the Skumanich relation to much faster rotation rates than it has been measured for (up to about 30 km/s). Recent indications are that the magnetic field generated by stellar dynamos saturates at $\Omega \gtrsim 10\Omega_\odot$, and therefore magnetic braking is probably (much) weaker at the rotation rates found in close binaries than implied by eq. (11.7).

By equating the loss of angular momentum with one or both of the mechanisms discussed above, we may use eq. (11.5) to calculate the evolution of a low-mass X-ray binary. Mass-transfer rates can be calculated this way for main-sequence stars, with $\zeta_{\rm eq} = 1$, and for white-dwarf donor stars, with $\zeta_{\rm eq} = -1/3$. If we assume the total mass of the binary to be conserved, then $\zeta_{\rm L}$ is given by eq. (7.22).[1] The results are shown in Figure 11.4, for angular momentum loss due to the emission of gravitational radiation only (eq. 11.5), and for the three types of donors given in Table 11.1, i.e. stars on the main sequence, stars on the helium main sequence, and white dwarfs.

For stars on the main sequence, the mass-transfer rate is about $\dot{M} \approx 10^{-10}\,M_\odot/{\rm yr}$, for donor masses between 0.2 and 1 $M_\odot$. Stars on the helium main sequence are smaller, and fill their Roche lobes in more compact binaries, leading to higher mass-transfer rates. Consider a main-sequence donor star. The mass transfer causes this star to become less massive, and the binary thus evolves towards shorter periods. At some point, the mass of the donor becomes too small to sustain significant hydrogen burning, and the core becomes degenerate. At this point, which is reached for a donor mass of about $0.08 M_\odot$, further mass loss of the donor causes it to expand. The orbit expands with it, according to eq. (11.2). Thus, the evolution of the orbital period passes through a minimum. Detailed calculations show that this minimum may be identified with the cutoff at around 80 min observed in the period distribution of cataclysmic variables.

A similar line of reasoning shows that binaries with donors that initially burn helium must also show a minimum period, which detailed calculations put at around 10 min.

The minimum period for a binary whose donor is a main-sequence star depends on the chemical composition of the core of this star. If its helium abundance is higher, the star is relatively more compact,

[1] Extension to the more general case is straightforward, using eq. (7.14) in combination with eq. (6.2).

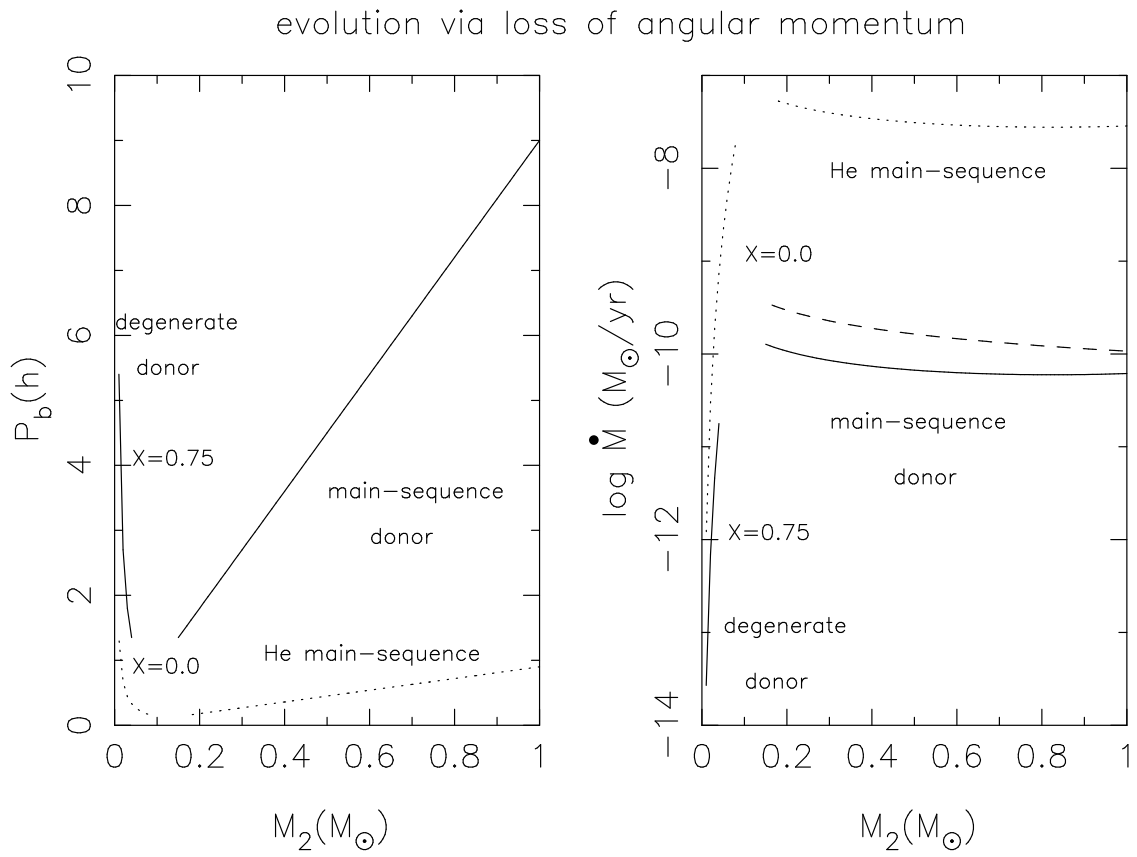

Figure 11.4. Orbital period and mass-transfer rate as a function of donor mass M_2, for binary evolution driven by loss of angular momentum via gravitational radiation. For degenerate donors (shown for $M_2 < 0.15 M_\odot$; solid and dashed lines for the indicated values of the hydrogen abundance) the orbital period increases and the mass-transfer rate drops precipitously, as the donor mass decreases. For main-sequence donors (shown for $M_2 > 0.15 M_\odot$; solid and dashed line for stars on the hydrogen and helium main sequence, respectively) the orbital period decreases and the mass-transfer rate hardly changes, as the donor mass decreases. The mass-transfer rates shown all assume $M_1 = 1.4 M_\odot$, except for the dashed line, which assumes that the mass receiver is a 7 $M_\odot$ black hole.

and becomes degenerate at a smaller radius. Thus, such binaries may evolve to periods shorter than 80 min. A main-sequence star with a helium-enriched core may be formed when the donor starts transferring mass to its companion near the end of its main sequence life. The mass loss stops further evolution of this donor star, which reverts to the main sequence, but with an enhanced He abundance in the core.

A number of low-mass X-ray binaries have X-ray luminosities well in excess of 10^{36} ergs, and hence mass accretion rates well in excess of $10^{-10}\ M_\odot$/yr, according to eq. (9.1). The orbital periods of several of these systems are too long for helium-burning donor stars, and more indicative of main-sequence donors. If one assumes that the currently observed $\dot{M}$ is also indicative of the $\dot{M}$ averaged over the time scale on which the binary evolves, such high mass-transfer rates require explanation. As suggested by eq. (11.4), any additional mechanism of loss of angular momentum increases the mass-transfer rate, and this has been the main reason to investigate mechanisms such as magnetic braking. The rate of angular momentum loss implied by eq. (11.7) is sufficiently high to explain the high observed values for mass-transfer rates in low-mass X-ray binaries and, less accurately, in cataclysmic variables. While magnetic braking is an attractive possibility to explain mass-transfer rates $\dot{M} \gtrsim 10^{-9}\ M_\odot$/yr in low-mass X-ray binaries with main-sequence-like donor stars, the details and actual efficiency of this process are not well understood. Furthermore, it is worthwhile to remark that many X-ray binaries have shown appreciable variability already during the few decades that X-ray observations have been possible, and to stress that therefore it is not possible to determine the long-term averaged values of $\dot{M}$. Therefore the importance

of magnetic braking in driving mass transfer in compact binaries has not been well-established.

11.3.2 Evolution via donor expansion

A number of low-mass X-ray binaries, including the well-known systems Sco X-1 and Cyg X-2, have orbital periods in excess of 0.5 days, indicating that their donor stars are (sub)giants (see Fig. 9.1). In these systems, mass transfer is driven by the evolutionary expansion of the donor star. The radius and luminosity of a low-mass giant are determined mainly by its core mass (see Fig. 6.3). Results of detailed calculations can be approximated by the core-mass radius relation given in Table 11.1, or more accurately with simple polynomial relations in $y \equiv \ln M_c/0.25M_\odot$:

$$\ln(R_\mathrm{d}/R_\odot) = a_0 + a_1 y + a_2 y^2 + a_3 y^3 \tag{11.8}$$

$$\ln(L_\mathrm{d}/L_\odot) = b_0 + b_1 y + b_2 y^2 + b_3 y^3 \tag{11.9}$$

The values of the fitting constants a_i, b_i depend on the metallicity of the star, and are given for two metallicities, for stars in the Galactic disk, and for stars in low-metallicity globular clusters, in Table 11.2.

The luminosity on the giant branch is almost completely due to hydrogen shell burning, and is related to the core mass M_c by

$$\dot{M}_c \approx 1.37 \times 10^{-11} \left(\frac{L}{L_\odot}\right) M_\odot/\mathrm{yr} \tag{11.10}$$

Combining eqs. (11.8) and (11.10) gives the relation between the change in radius and the change in core mass:

$$\frac{\dot{R}_\mathrm{d}}{R_\mathrm{d}} = [a_1 + 2a_2 y + 3a_3 y^2]\frac{\dot{M}_c}{M_c} \tag{11.11}$$

In the absence of loss of angular momentum, eq. (11.4) may be rewritten

$$-\frac{\dot{M}_\mathrm{d}}{M_\mathrm{d}} = \frac{1}{\zeta_\mathrm{eq} - \zeta_\mathrm{L}} \left(\frac{\dot{R}_\mathrm{d}}{R_\mathrm{d}}\right)_\mathrm{ev} \tag{11.12}$$

which completes the set of equations required to calculate the binary evolution. The orbital period and the two masses determine the radius of the giant via eq. (11.2) and hence its core mass via eq. (11.8); the core mass determines the rate of radius expansion via eq. (11.11), and with this the mass-transfer rate via eq. (11.12). Thus the evolution can be calculated without resort to complete stellar evolution codes.

The results are shown in Figure 11.5 for $Z = 0.02$, the metallicity of ordinary disk stars. It is seen that there is a strong correlation between orbital period and mass-transfer rate: in a binary with a long orbital period, only a large giant fills its Roche lobe, and a large giant evolves more rapidly.

The simple calculations hold for stars beyond the subgiant branch; for subgiants, eq. (11.10) does not apply. Eqs. (11.8) and (11.9) are valid for giants at thermal equilibrium. Detailed calculations show that this is a good approximation until the donor envelope has been almost fully exhausted.

Table 11.2. Constants for the fits to the core-mass - radius and core-mass - luminosity relations for low-mass giants, according to Webbink, Rappaport, & Savonije (1983).

	a_0	a_1	a_2	a_3	b_0	b_1	b_2	b_3	mass range
$Z = 0.02$	2.53	5.10	-0.05	-1.71	3.50	8.11	-0.61	-2.13	$0.16 < M_c/M_\odot < 0.45$
$Z = 0.0001$	2.02	2.94	2.39	-3.89	3.27	5.15	4.03	-7.06	$0.20 < M_c/M_\odot < 0.37$

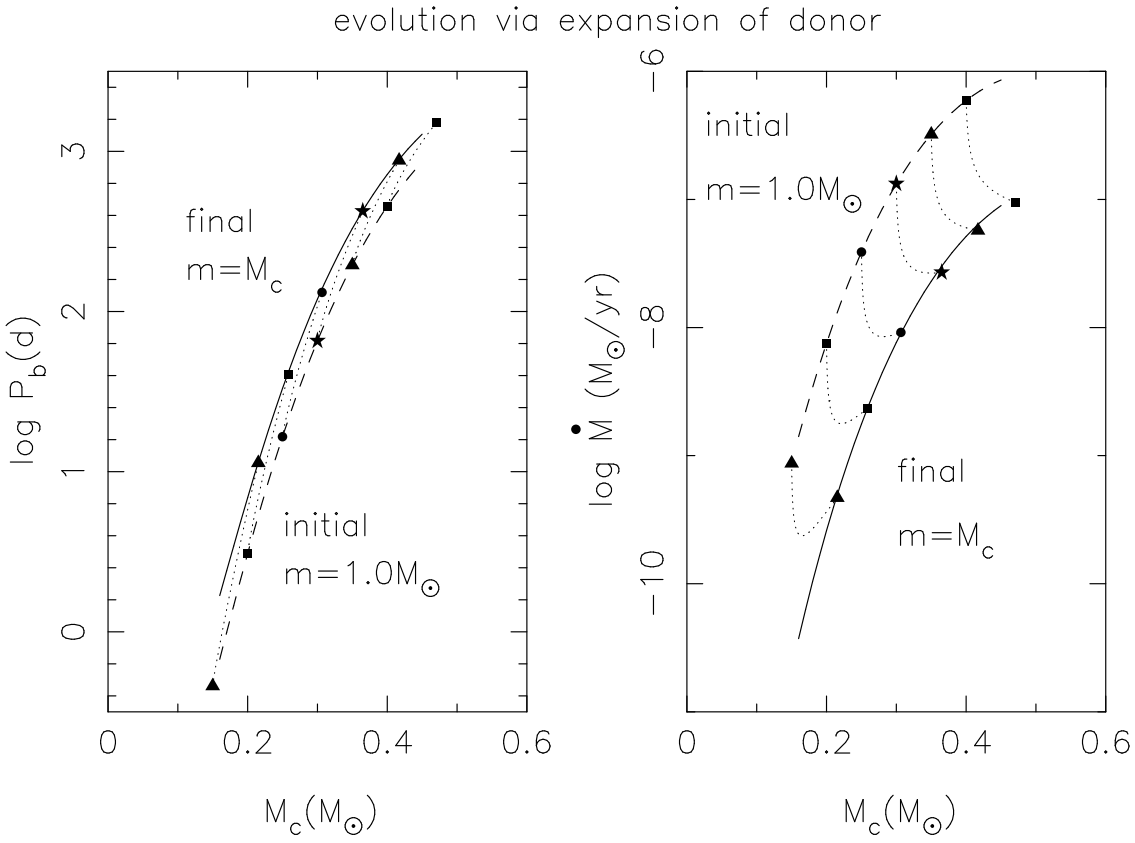

Figure 11.5. Orbital period and mass-transfer rate as a function of the mass of the donor core M_c, for binary evolution driven by expansion of a giant donor star. The mass-transfer rates shown all assume $M_1 = 1.4M_\odot$ and $\dot{M}_1 = -\dot{M}_2$.

11.3.3 Origin of low-mass binary radio pulsars

The evolutionary scenario for low-mass X-ray binaries with (sub)giant donors received strong confirmation with the discovery of radio pulsars in circular orbits with a very low mass-function, and hence a probable companion mass of $0.2 - 0.4M_\odot$ listed as low-mass binary radio pulsars in Table 9.5. The scenario discussed in the previous subsection automatically leads to such a binary: once the envelope of the giant donor is exhausted, the giant's core remains and cools into a white dwarf. The orbital period of the current binary sets the radius of the giant immediately prior to the end of mass transfer, and thus its core mass. Thus, the orbital period P_b of the radio pulsar should be correlated to the mass M_{wd} of its white-dwarf companion. Approximately (from Table 11.1):

$$P_{\rm orb} \approx 40\,{\rm days}\left(\frac{M_{\rm wd}}{0.25M_\odot}\right)^{5.5} \tag{11.13}$$

valid for for circular orbits with $P_b \gtrsim 20$ days.

The low eccentricity of the orbits of low-mass binary radio pulsars indicates that orbital circularization must have occurred following the formation of the neutron star. The low mass-functions indicate white dwarf companions to the radio pulsars with masses lower than the $\approx 0.6M_\odot$ expected for a white dwarf evolved from a single star. Both these observations are explained by the scenario in which a giant fills its Roche-lobe — causing strong tidal forces and hence rapid circularization, and transfers its envelope to the neutron star — thereby cutting off the growth of its core. The mass transfer also explains the short pulse period of the radio pulsars in these binaries as a consequence of the spin-up of the neutron star as it accretes mass from an accretion disk.

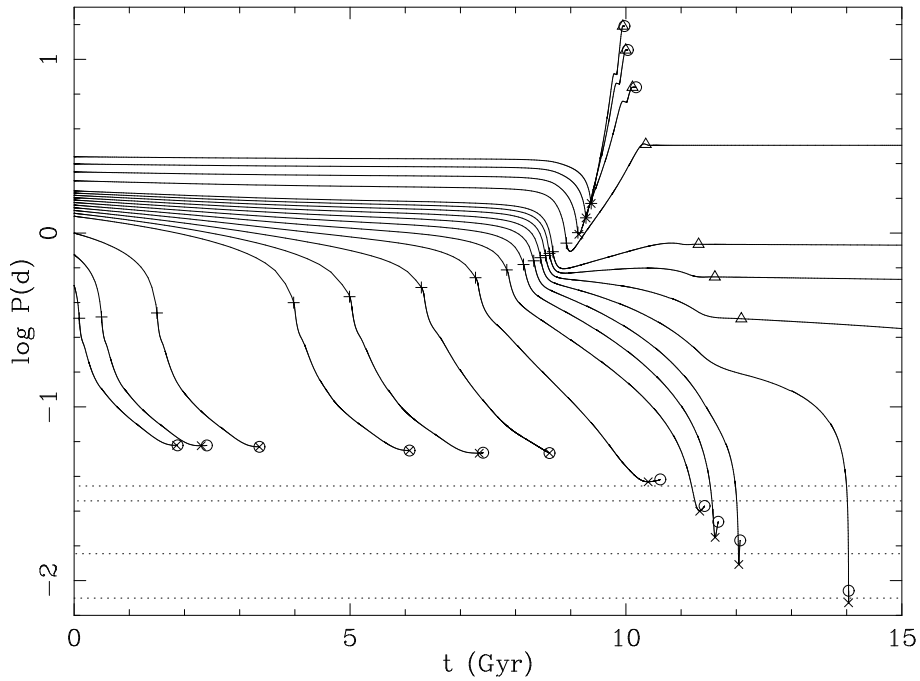

Figure 11.6. Evolution of the orbital periods of low-mass X-ray binaries with an initial donor mass of 1.0 $M_\odot$ and selected initial periods between 0.5 and 2.75 days. The curves show the results of detailed evolution calculations including angular momentum loss by gravitational radiation (eq. 11.5) as well as magnetic braking (eq. 11.7). The initial composition has $Z = 0.01$. The symbols mark special points in the evolution: + marks the start of Roche-lobe overflow (RLOF), $\times$ the minimum period, $\triangle$ the end of RLOF and $\bigcirc$ marks the end of the calculation. The four dotted horizontal lines show the orbital periods of the closest observed LMXBs in globular clusters: 11.4 and 20.6, and in the galactic disk: 41 and 50 minutes.
Systems with initial periods below the bifurcation period of about 1.5 days evolve to smaller orbital periods due to angular momentum loss (dominated by magnetic braking in this case) and mostly reach a minimum period of $\approx$ 70 min. Initially wider systems are dominated by nuclear expansion after the main sequence and evolve to longer periods. Systems with periods just below the bifurcation period develop helium-rich cores and can reach a minimum period as short as 10 min; however this requires strong fine-tuning of the initial period.

Interestingly, the realization that rapidly rotating radio pulsars may emerge from low-mass X-ray binaries came with the discovery of a single radio pulsar, PSR1937 + 21. Its extremely rapid rotation can be understood as the consequence of accretion of a substantial amount of mass $\gtrsim 0.1 M_\odot$ from an accretion disk, by a neutron star with a low magnetic field. The magnetic field of PSR1937 + 21 is indeed low (see Table 9.5). In order to explain the absence of any companion, several destruction mechanisms were suggested. Detailed scrutiny of these mechanisms showed that none of them are convincing. The discovery of another millisecond pulsar brought a more likely solution: PSR1957 + 20 is heating its companion enough to evaporate it.

11.3.4 Recent developments

Three recent developments are changing our picture of the low-mass X-ray binaries. First, it has been found that several low-mass X-ray binaries have donors with masses that aren't as low (viz. $\leq 1 M_\odot$) as hitherto assumed for low-mass X-ray binaries. For example, the black-hole binary GRO J 1655 – 40 has donor with a mass of about $2.3\,M_\odot$. It would appear that the donor must be a subgiant to fill its Roche lobe in the 2.6 d orbit. However, accurate radius determinations of main-sequence stars in double-lined eclipsing binaries show that stars with masses in the range 2-4 $M_\odot$ expand sufficiently on the main-sequence to explain mass transfer from a main-sequence star in GRO J 1655 – 40.

Secondly, the observation of black-hole binaries in low-mass systems with evolved donors implies that there are many times more – in the ratio of the main-sequence life time to the giant life time, i.e. a factor ~ 100 – black hole binaries with an unevolved companion which does not fill its Roche lobe. This has obvious consequences for the estimated birth rate of black-hole binaries.

And finally, the Wide Field Camera on board of the BeppoSAX X-ray satellite has discovered relatively dim X-ray transients, with peak luminosities $\leq 10^{37}$ erg/s, thanks to its unique combination of a large field of view and small angular separation. Most of these dim transients are bursters, i.e. neutron stars, which confounds the recent speculations that the vast majority of X-ray transients with low-mass donors are black hole systems.

Exercises

11.1 Consider the low-mass X-ray binary V4134 Sgr listed in Table 9.4. In this exercise, assume that the X-ray source is a neutron star (with $M = 1.4\,M_\odot$ and $R = 10$ km) and that the measured X-ray luminosity is the total accretion luminosity. Also assume the mass of the binary is conserved during mass transfer.

(a) Use the observed properties to compute the mass transfer rate in this system.

(b) Consider the orbital period of V4134 Sgr. Without doing any actual calculations, argue which of the following processes could be responsible for driving mass transfer in this system:

– nuclear expansion of the donor
– orbital angular momentum loss by gravitational radiation
– orbital angular momentum loss by magnetic braking
– exchange of orbital and spin angular momentum by tidal interaction.

(c) Compute the expected mass transfer rate if mass transfer is driven by (1) gravitational radiation, and (2) by magnetic braking. Compare your answers to the result you obtained for (a): which process is most likely to drive the observationally inferred mass transfer rate?

11.2 Now consider the low-mass X-ray binary Sco X-1, again referring to Table 9.4. Make the same assumptions as in exercise 11.1.

(a) Consider the various types of donor star summarized in Table 11.1. Which of these are possible donors of Sco X-1?

(b) Assume from now on that the donor is (just) on the red giant branch and has a mass of $1.0\,M_\odot$. Compute the expected mass transfer rate from nuclear expansion of the donor, and compare to the mass transfer rate inferred from its observed X-ray luminosity.

Note: instead of eqs. 11.8–11.9, you may also use the simpler (somewhat less accurate) relations between core mass, radius and luminosity given in Table 11.1 and

$$\frac{L}{L_\odot} = 2.3 \times 10^5 \left(\frac{M_c}{M_\odot}\right)^6$$

Bibliography

Gies, D. R., Bagnuolo, Jr., W. G., Ferrara, E. C., et al. 1998, ApJ, 493, 440
Hjellming, M. S. & Webbink, R. F. 1987, ApJ, 318, 794
Iben, I. J. & Livio, M. 1993, PASP, 105, 1373
Nelemans, G., Verbunt, F., Yungelson, L. R., & Portegies Zwart, S. F. 2000, A&A, 360, 1011
Nelson, C. A. & Eggleton, P. P. 2001, ApJ, 552, 664
Packet, W. 1981, A&A, 102, 17
Pols, O. R. 1994, A&A, 290, 119
Soberman, G. E., Phinney, E. S., & van den Heuvel, E. P. J. 1997, A&A, 327, 620
Tauris, T. M. & van den Heuvel, E. P. J. 2006, Formation and evolution of compact stellar X-ray sources (Compact stellar X-ray sources), 623–665
van der Sluys, M. V., Verbunt, F., & Pols, O. R. 2006, A&A, 460, 209
Webbink, R. F., Rappaport, S., & Savonije, G. J. 1983, ApJ, 270, 678
Weidemann, V. 1990, ARAA, 28, 103
Wellstein, S., Langer, N., & Braun, H. 2001, A&A, 369, 939